


Summer 7-3-2019

# AN ESTIMATION OF LOWER TROPOSPHERIC MIXING DERIVED FROM INVERSE MODELING OF BOUNDARY LAYER WATER VAPOR ISOTOPOLOGUES ON GRACIOSA ISLAND, AZORES

Jacquelyn M. Delp

*University of New Mexico Earth & Planetary Sciences*

Follow this and additional works at: [https://digitalrepository.unm.edu/eps\\_etds](https://digitalrepository.unm.edu/eps_etds)

 Part of the [Atmospheric Sciences Commons](#), [Climate Commons](#), [Geochemistry Commons](#), and the [Hydrology Commons](#)

---

## Recommended Citation

Delp, Jacquelyn M.. "AN ESTIMATION OF LOWER TROPOSPHERIC MIXING DERIVED FROM INVERSE MODELING OF BOUNDARY LAYER WATER VAPOR ISOTOPOLOGUES ON GRACIOSA ISLAND, AZORES." (2019).  
[https://digitalrepository.unm.edu/eps\\_etds/255](https://digitalrepository.unm.edu/eps_etds/255)

This Thesis is brought to you for free and open access by the Electronic Theses and Dissertations at UNM Digital Repository. It has been accepted for inclusion in Earth and Planetary Sciences ETDs by an authorized administrator of UNM Digital Repository. For more information, please contact [amywinter@unm.edu](mailto:amywinter@unm.edu).

Jacquelyn Delp

*Candidate*

Earth & Planetary Sciences

*Department*

This thesis is approved, and it is acceptable in quality and form for publication:

*Approved by the Thesis Committee:*

Dr. Joseph Galewsky, Chairperson

Dr. David Gutzler

Dr. Zachary Sharp

---

---

---

---

---

---

---

---

**AN ESTIMATION OF LOWER TROPOSPHERIC  
MIXING DERIVED FROM INVERSE MODELING OF  
BOUNDARY LAYER WATER VAPOR ISOTOPOLOGUES  
ON GRACIOSA ISLAND, AZORES.**

**by**

**JACQUELYN DELP**

**BACHELOR OF SCIENCE, UNIVERSITY OF FLORIDA**

THESIS

Submitted in Partial Fulfillment of the  
Requirements for the Degree of

**Master of Science  
Earth & Planetary Sciences**

The University of New Mexico  
Albuquerque, New Mexico

**May 2019**

## ACKNOWLEDGEMENTS

I would like to thank my advisor, Dr. Joseph Galewsky, for his dedication to my growth as a scientist during the last two years. His encouragement and mentorship has allowed me to develop skills in quantitative problem solving that I did not know I was capable of prior to coming to UNM. I feel very lucky to have worked with him for my master's degree.

Thank you to my committee members, Dr. David Gutzler and Dr. Zachary Sharp. I appreciate the time you spent teaching the courses I took for my master's degree, and I am especially grateful for the time you took to chat with me about my own research.

To Dr. Aurora Pun, thank you for helping me build my teaching skills for the two semesters I was able to serve as a teaching assistant for ENVS102L, and for providing me with career advice whenever I needed it.

Thank you to my fellow Earth & Planetary Sciences graduate students for your friendships and scientific support through the last two years. I am particularly grateful to Sebastian Los, who spent many hours working through research questions with me; Kristin Pearthree, who walked with me to get a countless number of Twisters burritos; Nels Bjarke, for providing my awkward dog-child with a friend that is your even more awkward dog-child; and Benjamin Holt, who helped me keep my sanity during an infinite number of inverse modeling problems by hiking up mountains with me.

Finally, thank you to my family for your encouragement and support throughout the last two years. I especially want to thank my grandpa, Dr. Charlie Delp, for his inspiration to be a good scientist, a good science communicator, and a good person.

**AN ESTIMATION OF LOWER TROPOSPHERIC MIXING DERIVED FROM  
INVERSE MODELING OF BOUNDARY LAYER WATER VAPOR  
ISOTOPOLOGUES ON GRACIOSA ISLAND, AZORES**

**By**

**Jacquelyn Delp**

**B.S., Geological Sciences, University of Florida, 2015**

**ABSTRACT**

Recent studies have shown water vapor isotopologues to be sensitive tracers of mixing processes that govern low-cloud feedback in climate models. In this study, we develop an inverse model (MBL Mix inverse model) that uses one year of isotope and humidity observations from Graciosa Island, Azores to estimate mixing for four seasons. We show the dry end-member of the model, the lower free troposphere (LFT), can be represented using Rayleigh fractionation. Isotope observations from Graciosa Island are compared to other field locations to discuss controls on isotopic variability other than mixing. Output from the MBL Mix inverse model shows the lowest (highest) fractions of seasonal-scale average mixing correspond to months previously observed to have the highest (lowest) occurrence of low-clouds. The model additionally shows a minimum mixing of approximately 0.3 is required to match observed data in all seasons in the Azores.

## TABLE OF CONTENTS

<b>LIST OF FIGURES .....</b>	<b>vii</b>
<b>LIST OF TABLES .....</b>	<b>viii</b>
<b>1. Introduction.....</b>	<b>1</b>
1.1 Climate Modeling Uncertainty and Low-Cloud Feedback .....	1
1.2 Atmospheric Hydrologic Studies and Water Vapor Isotopologues .....	2
<b>2. Background .....</b>	<b>5</b>
2.1 Importance of Modeling Processes Controlling Water Vapor Isotopologues.....	5
2.1.1 The Craig and Gordon Model.....	5
2.1.2 The MBL Mix Forward Model.....	7
2.2 Study Area.....	10
<b>3. Purpose of Study .....</b>	<b>12</b>
3.1 Describe MBL $\delta$ Variability on Graciosa Island, Azores.....	12
3.2 Introduce MBL Mix Inverse Model .....	12
3.3 Represent LFT Using Rayleigh Fractionation .....	13
3.4 Estimate Seasonal-Scale LFT Mixing on Graciosa Island, Azores .....	13
<b>4. Methods.....</b>	<b>15</b>
4.1 Isotope Analyzer Set-Up .....	15
4.2 Data Processing.....	16
4.2.1 Humidity-Induced Bias Correction .....	16
4.2.2 Calibration to International Standards.....	17
4.2.3 Standard Water Isotopic Composition Time Drift .....	18
4.2.4 Independent Verification of Humidity .....	19
4.3 Additional Instruments.....	20
4.4 MBL Mix Forward Model Sensitivity Tests .....	21
4.5 MBL Mix Inverse Model Set-Up .....	24
4.5.1 Constrain Input Parameters .....	24
4.5.2 Optimization Algorithm .....	25
<b>5. Results .....</b>	<b>28</b>
5.1 Observations from Graciosa Island .....	28
5.2 MBL Mix Inverse Model Calculations .....	37
<b>6. Discussion.....</b>	<b>44</b>
6.1 Comparison of Azores Observations to Other Study Areas.....	44

6.2 Benefits and Limitations of Rayleigh Fractionation .....	47
6.3 LFT Mixing Lower Bound .....	49
6.4 Seasonal-Scale LFT Mixing Variability and Low-Clouds.....	50
6.5 Uncertainty of MBL Mix Inverse Model .....	51
6.6 Advantage of Using Water Vapor Isotopologues in Addition to Humidity.....	56
<b>7. Conclusions.....</b>	<b>60</b>
<b>Appendix.....</b>	<b>63</b>
<b>References.....</b>	<b>71</b>

## LIST OF FIGURES

Figure 4.1: Humidity-induced bias correction surface fits for $\delta D$ and $\delta^{18}O$ .....	17
Figure 4.2: VSMOW-SLAP calibration surface fits for $\delta D$ and $\delta^{18}O$ .....	18
Figure 4.3: Specific humidity vs $\delta$ for MBL Mix curves showing sensitivity of the model to changes in LFT specific humidity and $\delta$ .....	22
Figure 4.4: Specific humidity vs $\delta$ for MBL Mix curves showing sensitivity of the model to changes in SST.....	23
Figure 5.1: Timeseries of $\delta D$ , $\delta^{18}O$ , d-excess, specific humidity, and SST for study .....	30
Figure 5.2: Seasonal observations of $\delta D$ with the closure assumption, a simple mixing model, and an MBL Mix model curve.....	34
Figure 5.3: Seasonal observations of $\delta^{18}O$ with the closure assumption, a simple mixing model, and an MBL Mix model curve .....	35
Figure 5.4: Seasonal observations of d-excess with the closure assumption, a simple mixing model, and an MBL Mix model curve .....	36
Figure 5.5: Seasonal comparison of observed and synthetic $\delta D$ contours.....	38
Figure 5.6: Seasonal comparison of observed and synthetic $\delta^{18}O$ contours .....	39
Figure 5.7: Seasonal comparison of observed and synthetic d-excess contours .....	40
Figure 5.8: Box plots of MBL Mix inverse model solved seasonal LFT mixing.....	42
Figure 5.9: MBL Mix Inverse Model Isotope-derived LFT Mixing versus RHS .....	43
Figure A.1: Box plots of MBL Mix inverse model solved seasonal initial Rayleigh fractionation $\delta D$ .....	65
Figure A.2: Box plots of MBL Mix inverse model solved seasonal initial Rayleigh fractionation $\delta^{18}O$ .....	65
Figure A.3: Box plots of MBL Mix inverse model solved seasonal LCL for Rayleigh fractionation .....	66
Figure A.4: Box plots of MBL Mix inverse model solved seasonal LFT specific humidity .....	66
Figure A.5: Box plots of MBL Mix inverse model solved seasonal LFT $\delta D$ .....	67
Figure A.6: Box plots of MBL Mix inverse model solved seasonal LFT $\delta^{18}O$ .....	67
Figure A.7: Box plots of MBL Mix saturation specific humidity of evaporative flux.....	68
Figure A.8: Box plots of MBL Mix inverse model solved seasonal ocean surface $\delta D$ ....	68
Figure A.9: Box plots of MBL Mix inverse model solved seasonal ocean surface $\delta^{18}O$ ..	69
Figure A.10: Box plots of MBL Mix inverse model solved seasonal MBL specific humidity .....	69
Figure A.11: Box plots of MBL Mix inverse model solved seasonal MBL $\delta D$ .....	70
Figure A.12: Box plots of MBL Mix inverse model solved seasonal MBL $\delta^{18}O$ .....	70



**LIST OF TABLES**

Table 4.1: Average Isotopic Composition of Secondary Standard Waters .....	19
Table 5.1: Graciosa Island Humidity and Isotope Observations .....	31
Table 5.2: NOAA SST Observations from Azores Region .....	32
Table 5.3: Goodness of Fit Statistics for MBL Mix Inverse Model Output .....	41
Table 5.4: MBL Mix Inverse Model Mixing Parameter .....	42
Table 5.5: LFT Mixing and RHS Quantitative Relations .....	43
Table 6.1: MBL Mix Inverse Model Mixing Variability .....	55
Table A.1: MBL Mix Inverse Model Parameters of Interest .....	64

## 1. Introduction

### 1.1 Climate Modeling Uncertainty and Low-Cloud Feedback

As the climate changes in response to the increasing atmospheric carbon dioxide (CO<sub>2</sub>) concentration, a number of feedbacks will act to enhance (positive feedback) or reduce (negative feedback) the average global temperature increase. Equilibrium climate sensitivity (ECS) modeling, the modeling of the increase in the average global temperature associated with doubling the atmospheric CO<sub>2</sub> concentration from pre-industrial levels, is a common approach for predicting future temperature change. The current spread of ECS generally falls between 1.5 and 4.5 K (IPCC, 2013). These estimates are reported with a relatively high uncertainty and a poorly constrained upper limit that has not been significantly improved since some of the earliest studies took place (Charney et al., 1979). Some feedbacks associated with climate change are well-constrained; however, others continue to be responsible for the uncertainty associated with ECS within an individual climate model as well as between different climate models (Bony and Dufresne, 2005; Sherwood et al., 2014).

Low-clouds have a particularly important feedback. They are generally thick, have a relatively broad extent and high albedo, and emit thermal radiation at temperatures close to the surface, allowing them to reflect a larger portion of incoming shortwave radiation than the longwave radiation they trap (Hartmann and Short, 1980; Bony and Dufresne, 2005; Barry and Chorley, 2010). These characteristics allow low-clouds to facilitate a net cooling effect on surface temperatures under current climate conditions.

In 2005, one study attributed a large source of uncertainty between climate models to differences in how they simulated the radiative effects of tropical low-clouds (Bony and

Dufresne, 2005). In 2012, another study reported the increase in upward force from increased ocean evaporation associated with climate change would drive a deeper, less moist near-surface atmosphere, resulting in less low-cloud cover and a positive feedback (Rieck et al., 2012). Sherwood et al. (2014) used output from 43 climate models to attribute 50% of the uncertainty in these models to differences in their simulated strength of the large- and small-scale convective mixing processes that govern low-cloud formation. This study demonstrated more mixing results in a decrease in the relative humidity of the marine boundary layer (MBL) and an increase in the relative humidity of the lower free troposphere (LFT), where low-cloud feedback was determined to be positive. These studies illustrate the importance of better understanding mixing between the MBL and LFT in order to better represent this process in climate models, simulate its influence on low-clouds, and produce more constrained estimates of likely future temperature conditions.

## **1.2 Atmospheric Hydrologic Studies and Water Vapor Isotopologues**

Isotopes have been used in hydrologic studies since the mid-1950s (Dansgaard, 1954). Hydrogen has two naturally occurring stable isotopes ( $^1\text{H}$  and  $^2\text{H}$ ;  $^2\text{H}$  is also referred to as D) and Oxygen has three naturally occurring stable isotopes ( $^{16}\text{O}$ ,  $^{17}\text{O}$ , and  $^{18}\text{O}$ ). The lightest isotopes are the most abundant, so most water molecules are comprised of the lightest isotopes of Hydrogen and Oxygen,  $^1\text{H}_2^{16}\text{O}$  (99.73098%). However, water molecules comprised of the heavier, rarer isotopes of Hydrogen and Oxygen,  $^1\text{H}_2^{18}\text{O}$ ,  $^1\text{H}_2^{17}\text{O}$ , and  $^1\text{HD}^{16}\text{O}$ , still occur at measurable quantities (Sharp, 2006).

The physical basis for using water isotopologues in hydrologic studies stems from the mass-dependent fractionation that takes place during phase change throughout the hydrologic cycle. Water molecules with heavier Oxygen or Hydrogen isotopes have greater

masses than those only composed of lighter isotopes, which causes them to have greater binding energies and lower diffusive velocities. Because evaporation and condensation are mass-dependent processes, phase change that occurs throughout the hydrologic cycle influences the isotopic composition of water vapor through the process of fractionation, and the resulting composition can provide unique information regarding atmospheric processes. Water molecules with heavier isotopes evaporate less readily and condense more readily compared to water molecules with light isotopes (Galewsky et al., 2016; Sharp, 2006).

Water vapor isotopologue compositions are reported as a ratio (R) of the concentration of the heavy isotope to the light isotope. This ratio is expressed relative to an international standard, the International Atomic Energy Agency (IAEA) Vienna Standard Mean Ocean Water (VSMOW), in the delta ( $\delta$ ) notation (McKinney et al., 1950) in units of per mil (‰) as expressed by **Equation 1.1**, where  $R_{\text{sample}}$  is the ratio of the sample and  $R_{\text{VSMOW}}$  is the ratio of the standard. Studies generally focus on two isotopes of water vapor,  $\delta\text{D}$  and  $\delta^{18}\text{O}$ , as well as the deuterium excess parameter, d-excess (Dansgaard, 1964). d-excess is calculated from the two isotopes, as expressed by **Equation 1.2** (Craig, 1961).  $\delta\text{D}$  and  $\delta^{18}\text{O}$  values that are less negative mean the sample is relatively enriched in the heavy isotope, while samples that are more negative are relatively depleted in the heavy isotope. d-excess is the result of a variety of kinetic processes that take place during the hydrologic cycle. Atmospheric water vapor  $\delta\text{D}$ ,  $\delta^{18}\text{O}$ , and d-excess measurements can provide useful information regarding the atmospheric hydrologic cycle by constraining the relative roles of phase change, transport, and mixing that are difficult to observe using humidity measurements alone (Galewsky et al., 2016).

**Equation 1.1**

$$\delta = \frac{R_{\text{sample}} - RVSMOW}{RVSMOW} \cdot 1000$$

**Equation 1.2**

$$\delta D = 8 \cdot \delta 180 + d - \text{excess}$$

## **2. Background**

### **2.1 Importance of Modeling Processes Controlling Water Vapor**

#### **Isotopologues**

Ocean evaporation is a critical component of the hydrologic cycle, due to moisture in the atmosphere originally being sourced from ocean evaporative flux. Because of this, some of the initial studies using water isotopologues put much effort into understanding the physical processes that control the  $\delta$  value of water vapor evaporating from the ocean. The original model describing the  $\delta$  values of water vapor evaporating from a water body was the Craig and Gordon Model (Craig and Gordon, 1965; described in **Section 2.1.1**), which was later simplified by Merlivat and Jouzel (Merlivat and Jouzel 1979; described in **Section 2.1.1**). More recent studies have used a combination of these previous models along with their own adaptations to better represent the  $\delta$  values of MBL water vapor measurements by representing mixing between the ocean evaporative flux and the LFT (Benetti et al., 2015, Benetti et al., 2018; described in **Section 2.1.2**).

#### **2.1.1 The Craig and Gordon Model**

The first comprehensive study of MBL water vapor isotopologues and their relation to evaporation and mixing was completed by Craig and Gordon (1965). This study used measurements from multiple ocean regions to show water vapor was more isotopically depleted than vapor in equilibrium with the sea surface. It demonstrated a strong correlation between isotopic composition and relative humidity (RH) calculated relative to saturation vapor pressure at sea surface temperature (SST). These observations were used to develop a three-layer model, where Layer 1 represented a liquid surface where condensation and evaporation occur, Layer 2 represented a laminar layer where molecular diffusion

dominates molecular transport rates, and Layer 3 was a turbulent layer where eddy diffusion and turbulent transport are the dominant processes. Processes taking place between layers were numerically represented with the Craig and Gordon Model, which calculates the  $\delta$  value of evaporated vapor using the  $\delta$  value of the liquid and surrounding free atmosphere, equilibrium fractionation at the vapor-liquid surface, RH normalized to saturation vapor pressure at the SST, deviation from equilibrium fractionation, and total kinetic isotopic effects derived from transport between the three layers.

The Craig and Gordon Model was later simplified by Merlivat and Jouzel (1979) where a parameter,  $k$ , was used to prescribe all kinetic effects by categorizing measurement conditions into a smooth (less than 6 or 7 m/s) or a rough (greater than 6 or 7 m/s) wind regime. Stronger fractionation is associated with the smooth wind regime. This study also proposed the closure assumption, further simplifying the Craig and Gordon Model by setting the  $\delta$  value of the evaporative flux equal to that of the entire MBL water vapor. This assumption refers to a closed water budget, where all vapor in the MBL is reasoned to be sourced from local evaporative flux, neglecting input from the LFT.

By using the closure assumption, MBL d-excess observations have successfully been reproduced (Benetti et al., 2014). However, the closure assumption predicts MBL  $\delta$  values that are less isotopically depleted than observations (Benetti et al., 2014; Jouzel and Koster, 1996; and Kurita, 2013). This can be explained by contribution to the MBL from a depleted air mass, such as the LFT. As altitude increases, water vapor becomes more isotopically depleted (Sharp, 2006), but d-excess remains relatively constant between the surface and mid-troposphere (Bony et al., 2008). This means mixing of LFT air into the MBL would not influence d-excess of the MBL while making MBL  $\delta$  values more

isotopically depleted, which is consistent with the above described observations. By releasing the closure assumption, modeling of MBL  $\delta$  values may potentially be used as tracers of mixing between ocean evaporation and the LFT (Benetti et al., 2018).

### 2.1.2 The MBL Mix Forward Model

Benetti et al. (2015 and 2018) investigated the controls of evaporation and mixing on MBL  $\delta$  values. They introduced a simple forward model that simulates MBL isotopic ratio as a result of mixing between a moist and dry end-member, where the moist end-member is represented by enriched ocean evaporative flux and the dry end-member is represented by depleted water vapor from the LFT. This results in a mixing curve that intersects observations of MBL water vapor isotopologues measured under stable atmospheric conditions.

The simplified mixing process is represented by **Equation 2.1**, where  $R_{MBL}$  is the isotopic ratio of the MBL,  $R_e$  is the isotopic ratio of evaporative flux from the ocean,  $R_{LFT}$  is the isotopic ratio of the LFT, and  $r$  is the LFT ratio (also referred to as LFT mixing hereafter). The LFT mixing represents the fraction of LFT moisture mixed into the MBL, as defined by **Equation 2.2**, where  $q_{LFT}$  is the specific humidity of the LFT and  $q_e$  is the specific humidity of the evaporative flux. Because the specific humidity of the MBL,  $q_{MBL}$ , is the result of mixing between the moist  $q_e$  and dryer  $q_{LFT}$ ,  $q_{MBL}$  is defined as the sum of fluxes from these parameters and  $r$  is equal to  $q_{LFT}/q_{MBL}$ .

**Equation 2.1**

$$R_{MBL} = (1 - r) \cdot R_e + r \cdot R_{LFT}$$

**Equation 2.2**

$$r = \frac{q_{LFT}}{q_e + q_{LFT}} = \frac{q_{LFT}}{q_{MBL}}$$

In **Equation 2.1**,  $R_e$  is defined using the above described Craig and Gordon Model, shown in **Equation 2.3**.  $R_{SW}$  is equal to the isotopic ratio of the ocean surface,  $\alpha_{eq}$  is the



temperature-dependent equilibrium fractionation factor, RHS is the relative humidity normalized to SST, and  $\alpha_k$  represents the kinetic fractionation factor. Because  $Re$  is a calculated parameter that includes the unknown parameter RMBL, **Equation 2.1 & 2.3** are combined and the resulting formula can be rewritten as **Equation 2.4**, where all known values are on the right side and the unknown RMBL is only on the left.

$$\text{Equation 2.3} \quad Re = \frac{\frac{RSW}{\alpha_{eq}} - (RHS \cdot RMBL)}{\alpha_k \cdot (1 - RHS)}$$

$$\text{Equation 2.4} \quad RMBL = \frac{\frac{(1 - r) \cdot RSW}{\alpha_{eq}} + r \cdot \alpha_k \cdot (1 - RHS) \cdot RLFT}{(1 - r) \cdot RHS + \alpha_k \cdot (1 - RHS)}$$

In the next step of the MBL Mix forward model, the LFT mixing is temporarily set equal to 0, briefly introducing the closure assumption to calculate the isotopic ratio of evaporative flux from the ocean. This allows the isotopic ratio of the evaporative flux to be iteratively calculated along a single MBL Mix curve based on changes in the specific humidity along the MBL Mix curve while still considering changes in the extent of mixing with the LFT. This iterative calculation allows the model to simulate a dynamic evaporative flux (a different isotopic ratio of the evaporative flux for each point along the mixing curve), which is shown by Benetti et al. (2018) to be a necessary step to better represent water vapor isotopologue observations than modeling exclusively with the closure assumption or by using a simple mass balance mixing model that does not consider a dynamic evaporative flux (Gedzelman, 1988; Galewsky and Hurley, 2010; Benetti et al. 2018). The calculation of the isotopic ratio of the evaporative flux with the closure assumption, listed below as RMJ79, is shown with **Equation 2.5**. Finally, by reorganizing

**Equation 2.4** as a function of RMJ79, **Equation 2.6** is obtained, which includes the parameter  $b$ , shown in **Equation 2.7**. In the last step of the calculation, the closure assumption is released, and the LFT ratio is no longer set equal to 0, allowing mixing to take place between RMJ79 and RLFT to represent conditions in the MBL.

$$\text{Equation 2.5} \quad RMBL \text{ (where } r = 0) = RMJ79 = \frac{\frac{RSW}{\alpha_{eq}}}{RHS + \alpha_k \cdot (1 - RHS)}$$

$$\text{Equation 2.6} \quad RMBL = (1 - b) \cdot RMJ79 + b \cdot RLFT$$

$$\text{Equation 2.7} \quad b = \frac{r \cdot \alpha_k \cdot (1 - RHS)}{(1 - r) \cdot RHS + \alpha_k \cdot (1 - RHS)}$$

There are two limitations of the MBL Mix model addressed in Benetti et al. (2015). (1) The model neglects horizontal advection. The authors of the 2015 study state that, in an oceanic setting, water vapor advected to a study location is the result of previous vertical mixing between ocean evaporative flux and the LFT in adjacent areas, meaning LFT water vapor is not necessarily from the LFT located directly above the study location. Because of this, water vapor from horizontal advection may experience different physical conditions (SST, atmospheric temperature, and wind) than those that are locally observed. However, the authors argue that on daily and longer timescales, regional conditions are relatively homogenous, meaning water vapor isotopologue changes associated with horizontal advection are small compared to those associated with vertical mixing. (2) The model considers instantaneous mixing, neglecting the residence time of water vapor within the MBL, assuming near surface water vapor is at a steady state. Despite these limitations, the MBL Mix model has initially demonstrated success reproducing the isotopic variability of MBL water vapor through accounting for vertical mixing and a dynamic evaporative flux

(Benetti et al., 2018). This means it can potentially be used with isotope and humidity observations to study, better understand, and improve simulation of the mixing dynamics that govern low-cloud feedback in climate models. In this paper, we argue an additional limitation of the MBL Mix forward model is that it does not offer a constrained estimate of LFT mixing that represents MBL isotope observations that lie along an MBL Mix curve; this study aims to improve this limitation (discussed in **Section 3.2**).

## 2.2 Study Area

This study uses one year of in-situ water vapor isotopologue measurements collected at the Department of Energy (DOE) Atmospheric Radiation Measurement (ARM) facility located on Graciosa Island, Azores. The Azores are a group of volcanic islands located at the triple junction of the North American, African, and Eurasian tectonic plates. Graciosa Island is the northernmost island within the central group of the Azores archipelago, located at approximately 39.1° North latitude and 28° West longitude. Low-clouds have an especially strong feedback over the ocean and previous studies have primarily focused on low-clouds in the subtropics. This means the Azores location in the transition between subtropical and midlatitude oceanic areas represents an opportunity to study the connection between water vapor isotopologues and mixing processes that determine low-cloud feedback in an underrepresented setting with different seasonal dynamics. Between September and March, this region is frequently crossed by the North Atlantic storm track and from late spring to summer the climate is influenced by the Azores anticyclone (Santos et al., 2004). The DOE ARM facility located on Graciosa Island presents the opportunity to complement water vapor isotopologue measurements to instruments capable of measuring changing atmospheric conditions. The position of the

DOE ARM facility on Graciosa Island is upwind from the climatologically prevailing winds and was chosen to reduce the island's effect on atmospheric measurements (Rémillard et al., 2012).

Although most studies focused on low-clouds have taken place in the subtropics, there has been some previous work focused on MBL clouds in the Azores. Rémillard et al. (2012) reported a 19-month long field campaign between June 2009 and December 2010 at the DOE ARM facility on Graciosa Island, which was the most extensive and comprehensive dataset of MBL clouds at the time. Wood et al. (2015) reported that the Azores position in the transition between the subtropical and midlatitude dynamic regimes makes this location particularly useful for observing cloud changes in dynamical transitions and testing the ability of models ranging from cloud-resolving to global climate models (GCMs) to simulate cloud changes.

### **3. Purpose of Study**

#### **3.1 Describe MBL $\delta$ Variability on Graciosa Island, Azores**

This study involved a one-year deployment to collect water vapor humidity and  $\delta$  data from Graciosa Island, Azores. We introduce the time series of these measurements and describe seasonal variability. We show observations of d-excess are generally well estimated by the closure assumption, but  $\delta D$  and  $\delta^{18}O$  are better represented by a model that consider mixing of LFT; we show MBL Mix has better success consistently estimating observations of  $\delta D$ ,  $\delta^{18}O$ , and d-excess compared to a simple mixing model that does not consider a dynamic evaporative flux (Gedzelman, 1988). Measurements from the Azores are additionally compared to observations from water vapor isotopic studies set in other ocean regimes.

#### **3.2 Introduce MBL Mix Inverse Model**

This study shows MBL Mix is the most recent model developed that consistently best fits MBL observations from the Azores. Because of this, we chose this forward model to adapt into an inverse model. While the forward model uses measurements of parameters controlling MBL  $\delta$  to generate a mixing curve that intersects observations of humidity and  $\delta$  values, the inverse model uses observed humidity and  $\delta$  values to estimate LFT mixing necessary to reproduce observations. It does this by pairing a stochastic forward model to a genetic algorithm which generates a best-fit solution of controlling parameters that can be used to create synthetic data points that match observations. Each synthetic data point has a known LFT mixing value which is used to represent the LFT mixing conditions of the observed data. This adaptation of MBL Mix from a forward model into an inverse

model advances the capabilities of this model by setting it up to provide a constrained estimate of LFT mixing.

### **3.3 Represent LFT Using Rayleigh Fractionation**

Measurements for this study were limited to near-surface in-situ observations, meaning  $\delta$  values in the LFT were not directly measured. Many studies do not have available instrumentation or resources to record observations in multiple locations simultaneously. In this study, we seek the simplest modelling approach that can still reproduce MBL  $\delta$  values by using the Rayleigh model of isotopic depletion (Dansgaard, 1964). This method provides an innovative approach to constrain the LFT for isotopic studies because a Rayleigh fractionation curve is generated using tools that would commonly be available at a wide variety of study locations and this approach allows LFT isotopic characteristics to be constrained without direct measurement.

### **3.4 Estimate Seasonal-Scale LFT Mixing on Graciosa Island, Azores**

Observations in the Azores were used with the MBL Mix inverse model to estimate LFT mixing for four seasons. We organize observations into March-April-May (MAM, Spring 2018), June-July-August (JJA, Summer 2018), September-October-November (SON, Fall 2018), and December-January-February (DJF, Winter 2018-2019). Each season of humidity and  $\delta$  observations are inversely modeled to develop distributions of each model-solved parameter, including LFT mixing. We compare LFT mixing between seasons to changes in seasonal atmospheric conditions as well as results from previous work (Rémillard et al., 2012) focused on low-cloud observations at the study area. By doing so, we demonstrate water vapor isotopologue and humidity measurement can be used

together to constrain the mixing processes that govern low-cloud formation and feedback that would be difficult to estimate only using humidity.

## 4. Methods

This study includes one year of water vapor isotopologue measurements from Graciosa Island, Azores. In this section, we go over the isotope analyzer set-up (**Section 4.1**), data processing techniques (**Section 4.2**), instruments other than the isotope analyzer that were used in this study (**Section 4.3**), sensitivities of the MBL Mix forward model (**Section 4.4**), and how the MBL Mix inverse model was designed (**Section 4.5**).

### 4.1 Isotope Analyzer Set-Up

Water vapor isotopologue and humidity measurements were determined using a Los Gatos Research (LGR) Triple Water Vapor Isotope Analyzer (TWVIA). This instrument was deployed from March 2018 through February 2019 at the DOE ARM facility located on Graciosa Island, where it was housed in a shipping container. The instrument was connected to an uninterruptable power supply and consists of three main components: a water vapor isotope analyzer, calibration unit, and dry air source.

Ambient air samples were collected through an inlet located several meters above the shipping container. Samples were then delivered to the analyzer through tubing by use of an external pump to optimize the transport time between the inlet and analyzer. The tubing within the shipping container was surrounded by a heating cable and insulating material to ensure ambient air samples did not fall below the dew point and result in condensation. The analyzer uses laser-based off-axis integrated cavity output spectroscopy to report isotopic ratios of ambient air samples in 10-second averages. The calibration unit of the instrument was used in conjunction with the dry air source to periodically measure the  $\delta$  values of standard waters. It uses a nebulizer to push small water droplets into a hot



chamber that vaporizes the water without fractionation. This vapor was then transported to the analyzer using a built-in compressor and the dry air source, which allows each standard with known  $\delta$  values to be measured at a wide range of humidity values for post-measurement calibration of ambient air samples.

## **4.2 Data Processing**

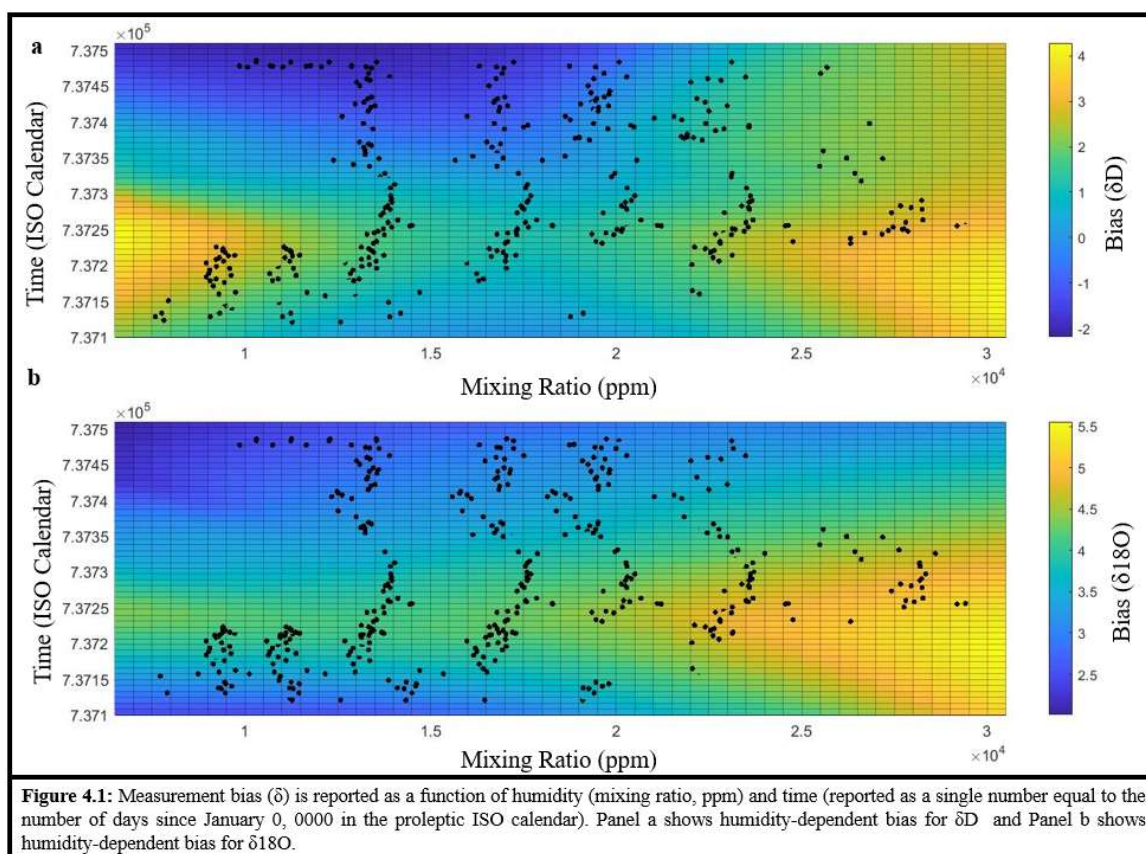
Multiple data processing steps were taken to account for humidity-induced bias, calibration to international standards, time drift in the  $\delta$  values of standard waters, and independent verification of the analyzer's humidity measurements (Galewsky et al., 2016).

### **4.2.1 Humidity-Induced Bias Correction**

A well-documented source of measurement bias is caused by the tendency of the analyzer to report isotope ratios as a function of humidity (Lis et al., 2008; Johnson et al., 2011). This relationship is generally found to be non-linear and unique to the individual isotope analyzer, the isotope ratio measured, and the humidity at which measurements are recorded (Lis et al., 2008; Bailey et al., 2015). Correcting for humidity-induced bias is highly important, as not doing so may lead to d-excess bias greater than 25‰ (Sturm and Knohl, 2010).

Three secondary standards (Deionized Water, Greenland Meltwater, and South Pole Meltwater) with a broad span of  $\delta$  values were deployed with the analyzer on Graciosa Island. Standards were run throughout the instrument's deployment at approximately 20-hour intervals, each of which included multiple periods of standard injections measured at mixing ratios spanning the range of local ambient humidity. Resulting measurements from Deionized Water were used to correct for the instrument's humidity-dependence by

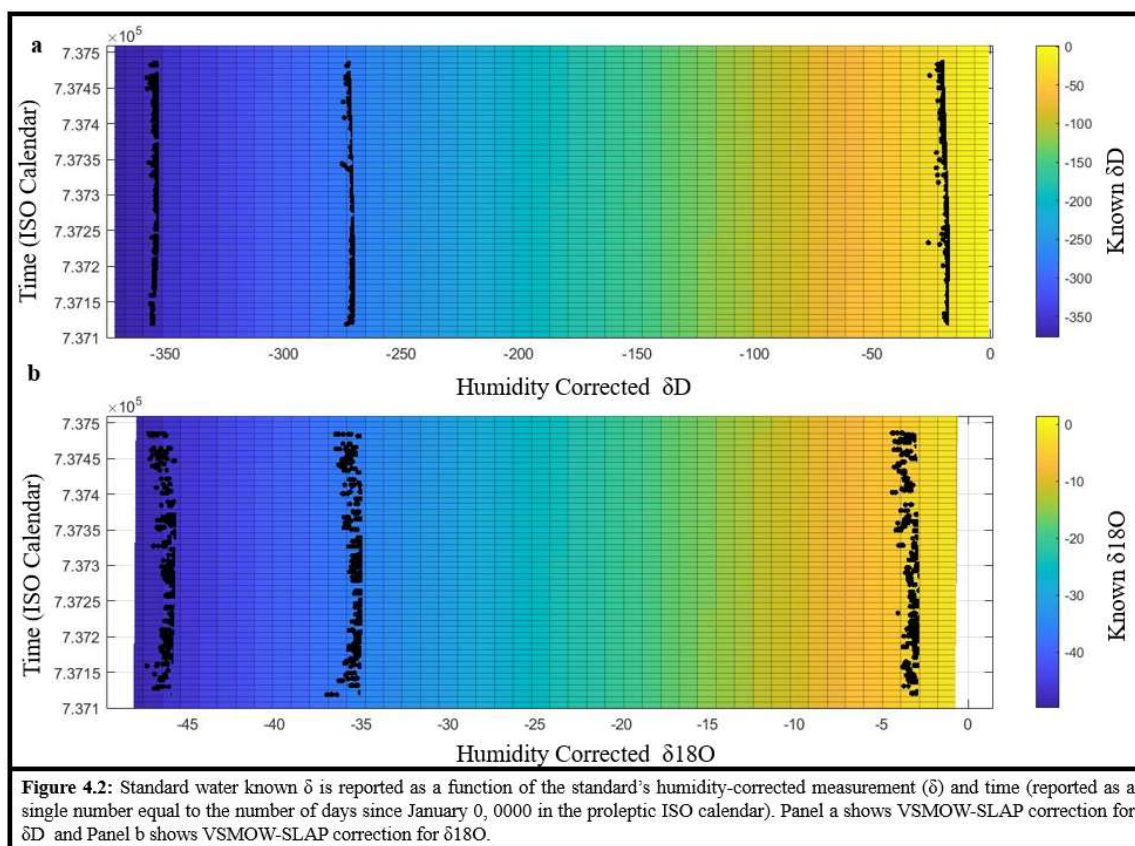
generating three-dimensional surface fits for  $\delta D$  and  $\delta^{18}O$ . The standard Deionized Water was chosen to generate this fit because its  $\delta$  values were closer to ambient air  $\delta$  values observed on Graciosa Island than the remaining secondary standards. The humidity-dependent surface fits plot bias (bias = known  $\delta$  – measured  $\delta$ ) as a function of mixing ratio and the time the standard was run (**Figure 4.1**), which corrects for humidity-induced bias as well as time drift in the analyzer's humidity-induced bias.



#### 4.2.2 Calibration to International Standards

After correcting for humidity-induced bias, the isotope observations must be calibrated to the international Vienna Standard Mean Ocean Water – Standard Light Antarctic Precipitation (VSMOW-SLAP) scale. This was accomplished by using

measurements from all three standard waters to generate surface fits for  $\delta D$  and  $\delta^{18}O$  plotting the known  $\delta$  value as a function of the humidity corrected  $\delta$  value and the time at which the standard water was measured (**Figure 4.2**). By incorporating time in the surface fits, long-term variability in the instrumental VSMOW-SLAP scale could be accounted for in the calibration of ambient air observations (Steen-Larsen et al., 2014).



### 4.2.3 Standard Water Isotopic Composition Time Drift

Time drift in the  $\delta$  values of standard waters was monitored throughout the analyzer's deployment. Some degree of change was expected due to fractionation associated with partial evaporation occurring during periodic opening and closing of standard water storage containers and bubbling of air into the water during the purge cycle

of the calibration unit during standard water injections. Changes in the isotopic composition of standard waters was mitigated by storing waters in large volumes, decreasing the overall effect of fractionation. Standard waters were measured periodically throughout the field deployment and recorded changes were found to be within analytical uncertainty. Because of this, an average value was calculated for each standard's  $\delta$  values (Table 4.1) and the average was used for the above described humidity-induced bias correction and VSMOW-SLAP calibration.

<b>Table 4.1: Average Isotopic Composition of Secondary Standard Waters</b>		
<b>Secondary Standard</b>	<b><math>\delta D</math> (‰)</b>	<b><math>\delta^{18}O</math> (‰)</b>
<b>Deionized Water</b>	-18.2	-2.94
<b>Greenland Meltwater</b>	-271.8	-35.10
<b>South Pole Meltwater</b>	-357.7	-46.00

**Table 4.1:** To account for time-drift, the isotopic composition of three secondary standard waters was measured multiple times throughout the isotope analyzers deployment in the Azores. Any recorded time-drift was found to be within analytical uncertainty. The above values are averages from the different measurements times and are the values used to complete the humidity-induced bias correction and VSMOW-SLAP calibration.

#### 4.2.4 Independent Verification of Humidity

The isotope analyzer's humidity measurements are compared to those recorded by the DOE ARM facility's meteorological station (met station). The isotope analyzer reports humidity in mixing ratio using units of parts per million (ppm) while the ARM met station records relative humidity, pressure, and temperature, which is converted to mixing ratio for comparison. During the field deployment, there was an average percent difference between the met station mixing ratio and the analyzer's mixing ratio of 3.8%.

### 4.3 Additional Instruments

The isotope analyzer's humidity and water vapor isotopologue measurements were paired with a variety of instruments located at the DOE ARM facility on Graciosa Island as well as National Oceanic and Atmospheric Administration (NOAA) satellite data. Because many instruments recorded at different time intervals, measurements were paired with the isotope observations through interpolation followed by time averaging all measurements. This study uses 3-hour averages. The purpose of pairing all instruments was to independently verify the humidity observations of the isotope analyzer (as described in **Section 4.2.4**) and document the changing environmental conditions that may be influencing the isotope and humidity observations for modeling purposes.

The DOE ARM facility on Graciosa Island launched twice-daily weather balloon soundings using Vaisala instrumentation that measured the vertical profile of the atmosphere's thermodynamic state as well as wind speed and direction. This study uses weather balloon sounding pressure, temperature, and relative humidity measurements.

The met station located at the DOE ARM facility has a variety of sensors that record atmospheric pressure, temperature, relative humidity, vapor pressure, precipitation rate, vector-averaged wind speed, and vector-averaged wind direction. These measurements are recorded in one-minute averages and have associated uncertainties of 0.1 kPa, 0.1 °C, 0.1 %, 0.1 kPa, 0.01 mm/hour, 0.1 m/second, and 1°, respectively.

This study uses NOAA's Earth System Research Lab Physical Science Division optimum interpolation satellite SST data (NOAA High Resolution SST). This product also uses data from ships and buoys and includes large-scale adjustment of satellite data with

respect to the in-situ data (Reynolds et al., 2007) Observations are recorded as daily averages on a  $0.25^\circ$  latitude by  $0.25^\circ$  longitude global grid.

#### 4.4 MBL Mix Forward Model Sensitivity Tests

Before setting up the MBL Mix inverse model and attempting to fit isotope and humidity observations from the Azores with inverse model output, this study explores the sensitivity of the MBL Mix forward model to input parameters. This is done by perturbing each of the individual input parameters while holding all others constant to a reference case. The input parameters for the MBL Mix forward model include: LFT specific humidity, LFT  $\delta D$  and  $\delta^{18}O$ , SST, ocean surface  $\delta D$  and  $\delta^{18}O$ , kinetic fractionation factors for  $\delta D$  and  $\delta^{18}O$ , and surface pressure. These tests revealed the MBL Mix forward model is particularly sensitive to changes in the LFT and SST.

**Figure 4.3** illustrates the forward model's response to changes in the humidity and  $\delta$  values of the LFT. Although changes in the LFT  $\delta$  values primarily influence the slope of less moist half of the curve, changes to the LFT specific humidity have a large effect on the slope of the entire MBL Mix forward model curve. LFT specific humidity is additionally highly influential in the calculation of LFT mixing ( $r$ , **Equation 2.2**) because it appears in both the numerator and denominator of this ratio. Because this study does not include direct measurements of the LFT characteristics, the dry endmember is estimated using the Rayleigh model of isotopic depletion (discussed further in **Section 4.5.1**).

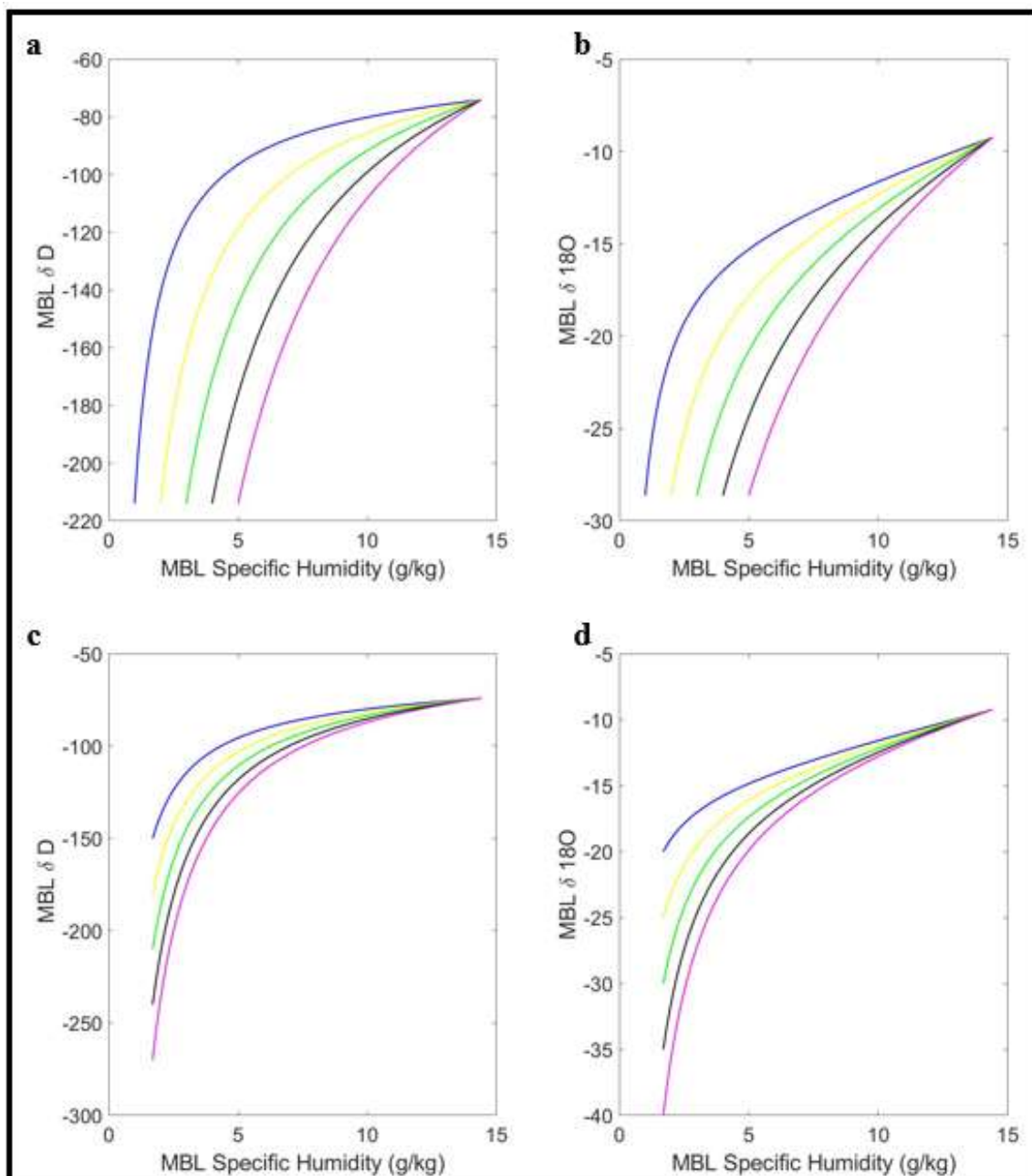
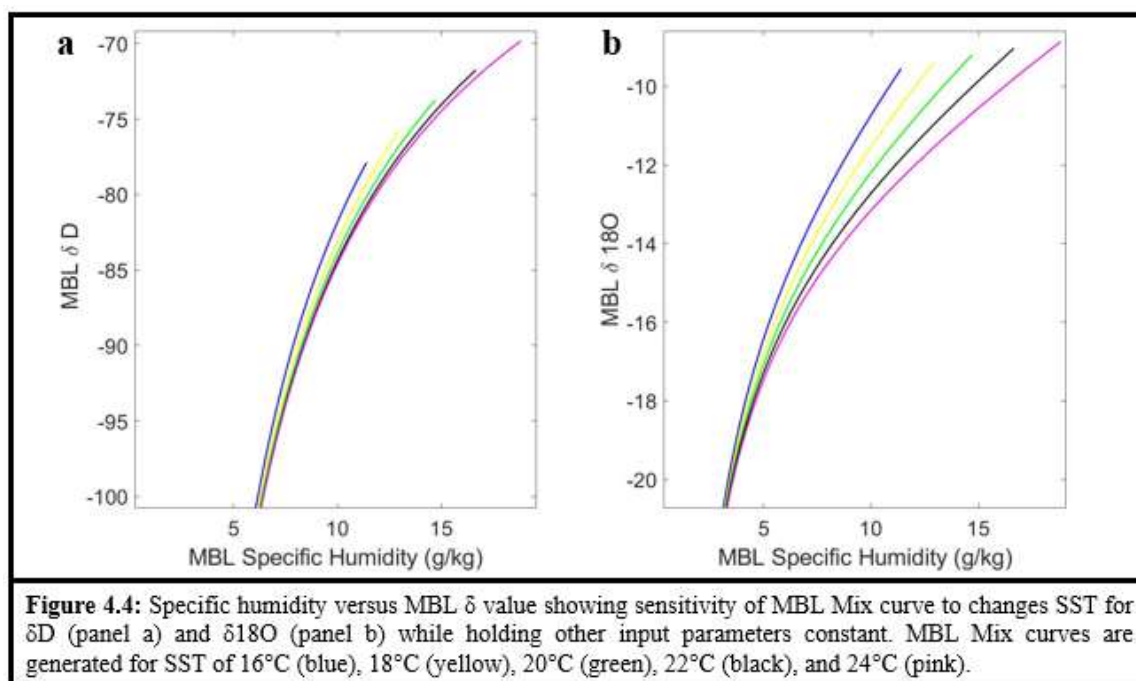


**Figure 4.3:** Specific humidity versus MBL  $\delta$  value showing sensitivity of MBL Mix curve to changes in LFT specific humidity (panel a and b) and changes in LFT  $\delta$  values (panel c and d) while holding other input parameters constant. In panels a and b, MBL Mix curves are generated for LFT specific humidity of 1 g/kg (blue), 2 g/kg (yellow), 3 g/kg (green), 4 g/kg (black), and 5 g/kg (pink). In panels c and d, MBL Mix curves are generated for LFT  $\delta D$  -150 and  $\delta 18O$  -20 (blue),  $\delta D$  -180 and  $\delta 18O$  -25 (yellow),  $\delta D$  -210 and  $\delta 18O$  -30 (green),  $\delta D$  -240 and  $\delta 18O$  -35 (black), and  $\delta D$  -270 and  $\delta 18O$  -40 (pink).

**Figure 4.4** illustrates the forward model's response to changes in SST. Changes to this parameter primarily influence the more humid half of the mixing curve because of its effect on the maximum specific humidity at which water vapor can evaporate from the ocean surface. Like changes to the LFT specific humidity, this also has an influence on  $r$ . To a lesser extent, there is an effect on the MBL  $\delta$  values. This is due to the use of SST to calculate the temperature-dependent equilibrium fractionation factor which is used to determine the  $\delta$  values of ocean evaporative flux. It is also due to the use of SST to calculate relative humidity normalized to SST, which contributes to determining MBL  $\delta$  values after mixing between the LFT and evaporative flux. Due to the sensitivity of the MBL Mix model to this parameter, this study splits the one year of observations from Graciosa Island into four seasons for individual analysis using the MBL Mix inverse model. By doing so, this allows the inverse model to use a more limited range of SST per season to generate synthetic points to match the observations.





## 4.5 MBL Mix Inverse Model Set-Up

This study seeks the simplest inverse model set-up that can reproduce observed humidity and  $\delta$  value trends in the MBL. Input parameters are constrained using a variety of methods described in **Section 4.5.1** and the inverse model is generated by use of a genetic algorithm described in **Section 4.5.2**. Each model unknown is given an upper and lower bound that the genetic algorithm uses to converge on an optimal solution within the specified range for that model parameter.

### 4.5.1 Constrain Input Parameters

LFT characteristics are not directly measured during this study and are instead constrained using the Rayleigh model of isotopic depletion (Dansgaard, 1964). This framework considers the idealized progressive effects of fractionation on a precipitating air parcel, where water vapor that condenses is immediately removed from the system. This leads to a dry and isotopically depleted air mass, which can be used to represent the LFT. In order to calculate a Rayleigh fractionation curve, we use the twice-daily weather balloon soundings to calculate an average temperature profile for each season. The average temperature profile is used to calculate a vertical profile of temperature-dependent equilibrium fractionation factors. Because initial delta values are unknown, we allow the genetic algorithm to solve for a beta distribution of initial delta values that includes range of observed  $\delta$  values on Graciosa Island. We additionally allow the genetic algorithm to solve for a beta distribution of lifting condensation levels in the atmosphere, which controls the humidity and equilibrium fractionation factor at which Rayleigh fractionation begins from the initial delta value. This generates a Rayleigh curve, from which the inverse model selects a best-fitting point to represent the LFT specific humidity and  $\delta$  values.

SST is constrained using NOAA satellite data. We use daily averages from latitude ranges 38.5° to 39.25° North and longitude ranges 27° to 29° West to index the ocean region surrounding Graciosa Island. Observations are used to generate a normal distribution for the inverse model. Ocean surface  $\delta$  values were also not directly measured during this period. We constrain ocean surface  $\delta D$  and  $\delta^{18}O$  with data collected from cruises between 2012 and 2015 (Benetti et al., 2017) by using the range of observed values to set upper and lower bounds for the inverse model to solve for a beta distribution within.

The final input parameters to constrain include surface pressure and the kinetic fractionation factors for  $\delta D$  and  $\delta^{18}O$ . This study uses averaged surface pressure observations collected by the met station at the DOE ARM facility. This study uses a calculation of the kinetic fraction factors consistent with Benetti et al. (2015), where fractionation is dependent on a smooth or rough wind speed regime (Merlivat and Jouzel, 1979). The average wind speed for each season fell within the smooth regime (kinetic fractionation factor for  $\delta D = 1.0053$  and  $\delta^{18}O = 1.0006$ ), which was input to the inverse model.

#### **4.5.2 Optimization Algorithm**

A genetic algorithm is an optimization algorithm that uses concepts from evolutionary biology (Beasley et al. 1993a,b). This study uses MATLAB's genetic algorithm function to solve for an optimized combination of unknown parameters (LFT specific humidity and  $\delta$  values, Ocean surface  $\delta$  values, LFT mixing, and Rayleigh fractionation's initial  $\delta$  values and lifting condensation level) that can be used to generate synthetic data points that best match observational data points. The genetic algorithm creates an initial generation of individual potential solutions, each of which has an

associated error. The genetic algorithm then uses those potential solutions as parents to produce new potential solutions as children for the next generation by implementing selection, crossover, and mutation. This is done iteratively until the genetic algorithm converges on the solution with the lowest error; this is the solution that generates synthetic data points that best match observed data points. Previous success with this method has been shown by Galewsky and Rabanus (2016), where inverse modeling of water vapor isotopologues with a genetic algorithm was successfully used to constrain last saturation and mixing parameters that govern subtropical humidity, and by Galewsky (2018), where inverse modeling with a genetic algorithm was used to demonstrate the first link between lower-tropospheric mixing, low-clouds, and isotope-derived mixing estimates.

Within the genetic algorithm, error is evaluated using a two-dimensional Kolmogorov-Smirnov test (referred to as K-S statistic; Peacock, 1983). This is a method which calculates error by using the largest absolute difference in the cumulative probability distributions between the synthetic and observed data's humidity and  $\delta$  values. Each season of observed data was evaluated with the MBL Mix inverse model multiple times using standardized conditions, to determine which model set-up yielded the lowest K-S statistic error. The standardized conditions used to determine best-fit conditions include adjusting both the population size of each generation of the genetic algorithm (we evaluated model error using population sizes of 2000 and 3000) as well as the upper bound of the alpha and beta values used to generate the beta distribution of each parameter optimized by the genetic algorithm (we evaluate model error using alpha and beta value upper bounds of 25, 50, and 100). The combination of population as well as alpha and beta value adjustments

that yielded the output with the lowest error for each season was selected to present as the results of this study.

## 5. Results

### 5.1 Observations from Graciosa Island

3-hour averaged humidity and isotope observations from the 12-month measurement period are illustrated on **Figure 5.1** (panels a – d). These measurements are organized on **Table 5.1** using the mean and standard deviation for the entire data set (One Year 2018 - 2019) as well as the individual seasons (MAM 2018, JJA 2018, SON 2018, and DJF 2018 – 2019). There are four sources of uncertainty introduced at different stages during the data collection and processing. These include (1) instrument precision, (2) uncertainty in the secondary standards, (3) humidity-correction uncertainty, and (4) VSMOW-SLAP calibration uncertainty. Uncertainty from each step is propagated in quadrature to calculate a total uncertainty of each isotopologue. Uncertainty was determined to be 1.8‰ for  $\delta D$  and 0.95‰ for  $\delta^{18}O$ .

The annual averages for  $\delta D$  and  $\delta^{18}O$  were -87.7‰ and -12.98‰, respectively.  $\delta D$  ranged between -156.4‰ and -67.5‰, and  $\delta^{18}O$  ranged between -20.93‰ and -8.49‰. On the seasonal scale, JJA had the highest average MBL  $\delta$  value (-84.1‰) while DJF had the lowest (-94.9‰). The highest variability (standard deviation) in MBL  $\delta$  values was observed in DJF for both  $\delta D$  (13.5‰) and  $\delta^{18}O$  (2.03‰), while the least variability in  $\delta D$  was observed in SON (7.9‰) and least variability in  $\delta^{18}O$  was observed in JJA (1.40‰). The annual average for d-excess was 16.1‰ with a standard deviation of 8.1‰. d-excess ranged between -19.5‰ and 41.0‰ during the deployment period. On the seasonal scale, average MBL d-excess was observed to be highest (18.8‰) and the least variable (1.7‰) during DJF and the lowest (13.1‰) during JJA with moderate variability (5.2‰). MAM

and SON had d-excess averages and standard deviations similar to that of the annual scale. The annual average and standard deviation of MBL specific humidity was 10.2 g/kg and 3.0 g/kg, respectively. MBL specific humidity ranged between 4.5 g/kg and 17.3 g/kg during the study period. On the seasonal scale, JJA had the highest average MBL specific humidity (12.7 g/kg) while MAM had the lowest (8.0 g/kg), which was closely followed by DJF (8.2 g/kg). DJF had the least variability of MBL specific humidity (1.7 g/kg) while SON had the most (2.8 g/kg).

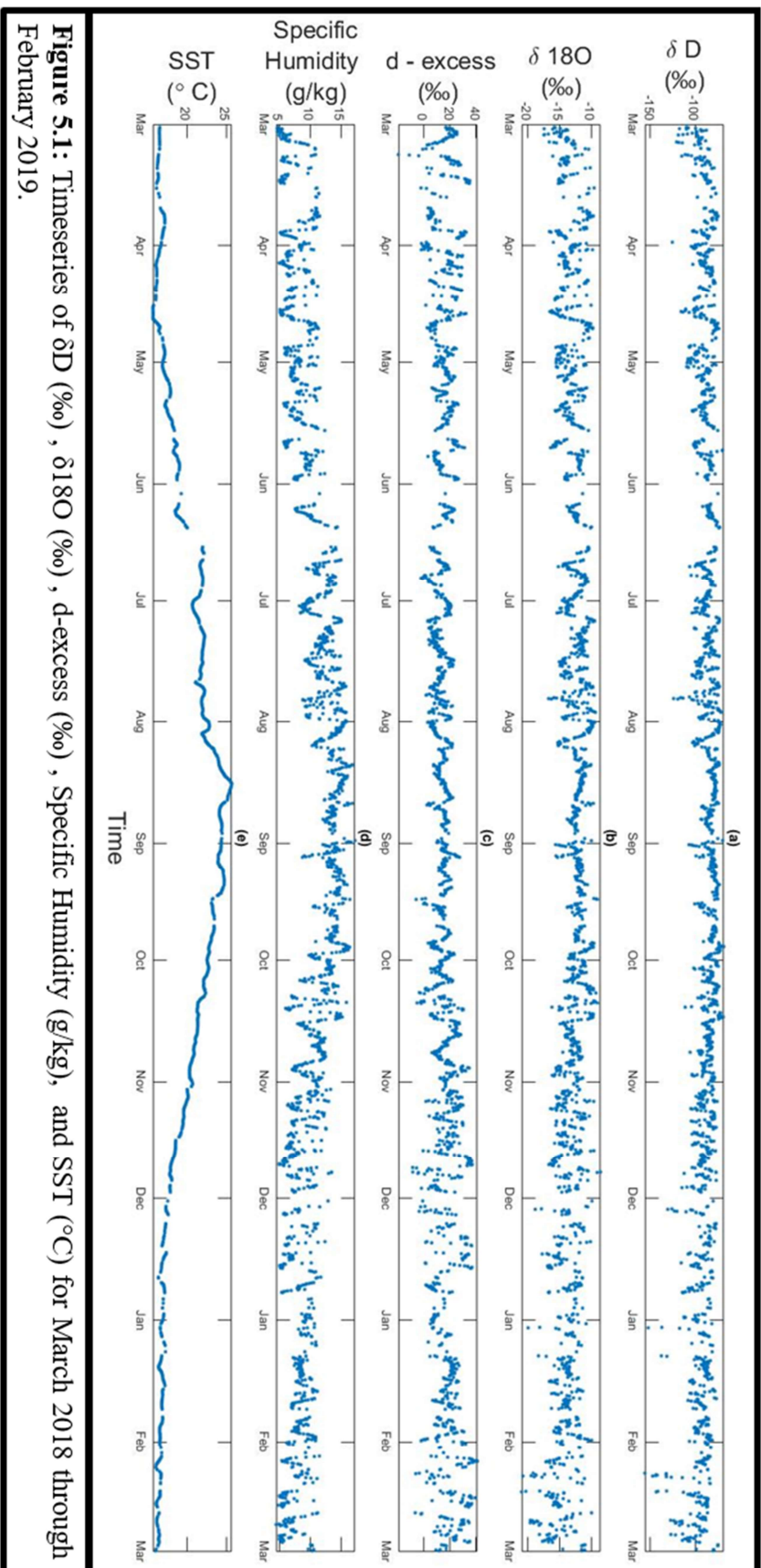


**Figure 5.1:** Timeseries of  $\delta D$  (‰),  $\delta 18O$  (‰), d-excess (‰), Specific Humidity (g/kg), and SST (°C) for March 2018 through February 2019.

Time Period	Specific Humidity (g/kg)		$\delta D$ (‰)		$\delta^{18}O$ (‰)		d - excess (‰)	
	Mean	St.Dev	Mean	St.Dev	Mean	St.Dev	Mean	St.Dev
One Year (2018 - 2019)	10.2	3.0	-87.7	10.5	-12.98	1.83	16.1	8.1
MAM (2018)	8.0	2.0	-89.6	9.2	-13.24	1.70	16.9	8.2
JJA (2018)	12.7	2.1	-84.1	8.2	-12.16	1.40	13.1	5.2
SON (2018)	11.1	2.8	-84.6	7.9	-12.66	1.61	16.7	8.0
DJF (2018 - 2019)	8.2	1.7	-94.9	13.5	-14.22	2.03	18.9	1.7

Table 5.1: Mean and standard deviation for specific humidity,  $\delta D$ ,  $\delta^{18}O$ , and d-excess data collected using LGR TWVTA on Graciosa Island, Azores from March 1, 2018 until February 28, 2019. Measurements are reported for the entire time series (one year) as well as four seasons (MAM, JJA, SON, and DJF) within the one year deployment.



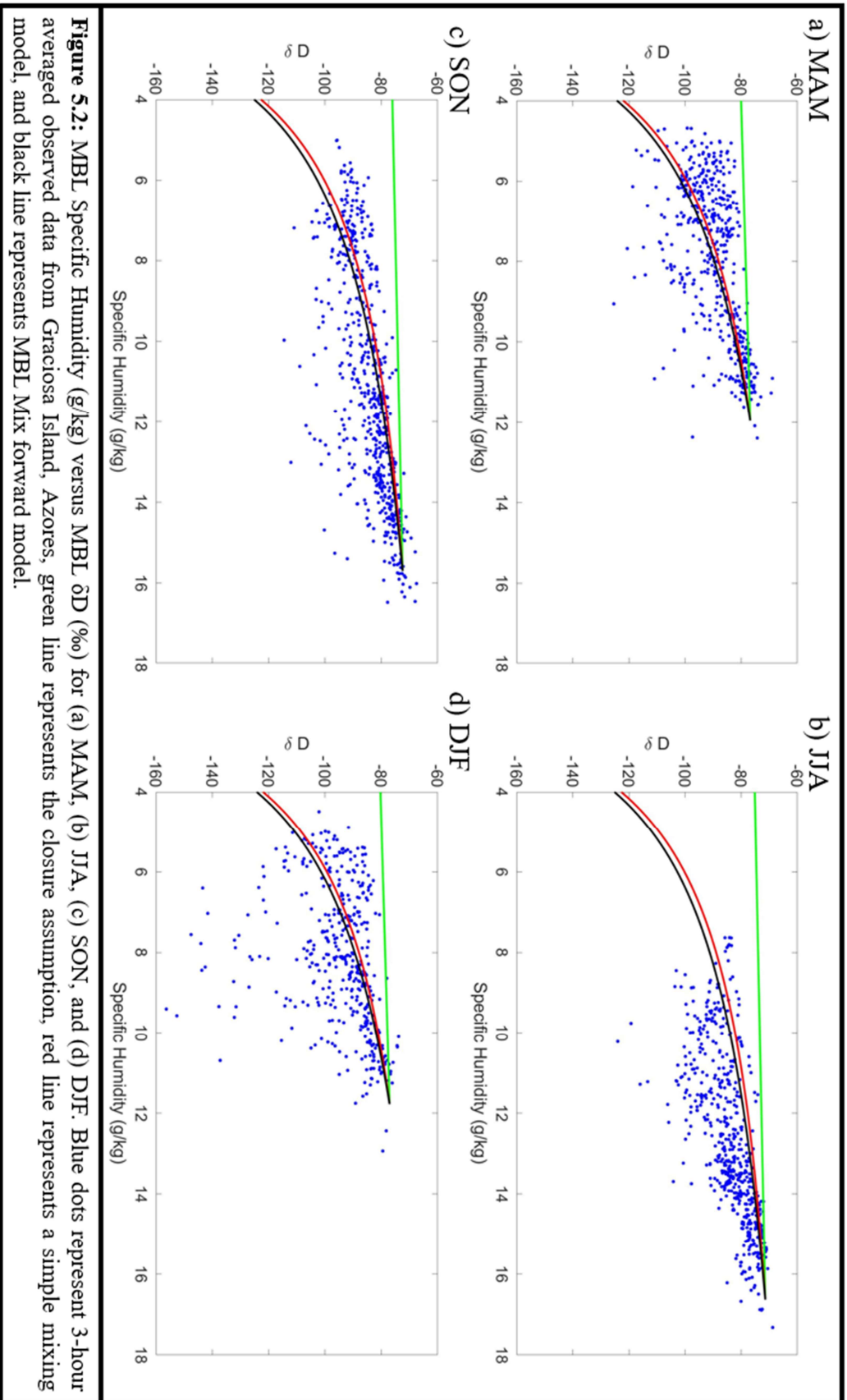
NOAA SST observations from the measurement period are illustrated on **Figure 5.1** (panel e) and reported on **Table 5.2** using the mean and standard deviation for the entire year and each season. The annual average SST was 19.7°C and the standard deviation was 2.9°C. During the study period, SST ranged between 15.7°C and 25.7°C. On the seasonal scale, average SST was observed to be warmer than the annual average in JJA (22.4°C) and SON (21.3°C), but colder than average in MAM (17.0°C) and DJF (16.8°C). SON had the most variability in SST (2.0°C) while DJF had the least (0.3°C).

<b>Table 5.2: NOAA SST Observations from Azores Region</b>		
<b>Time Period</b>	<b>SST (degree C)</b>	
	<b>Mean</b>	<b>St.Dev</b>
<b>One Year (2018 - 2019)</b>	19.7	2.9
<b>MAM (2018)</b>	17.0	1.6
<b>JJA (2018)</b>	22.4	1.6
<b>SON (2018)</b>	21.3	2.0
<b>DJF (2018 - 2019)</b>	16.8	0.3

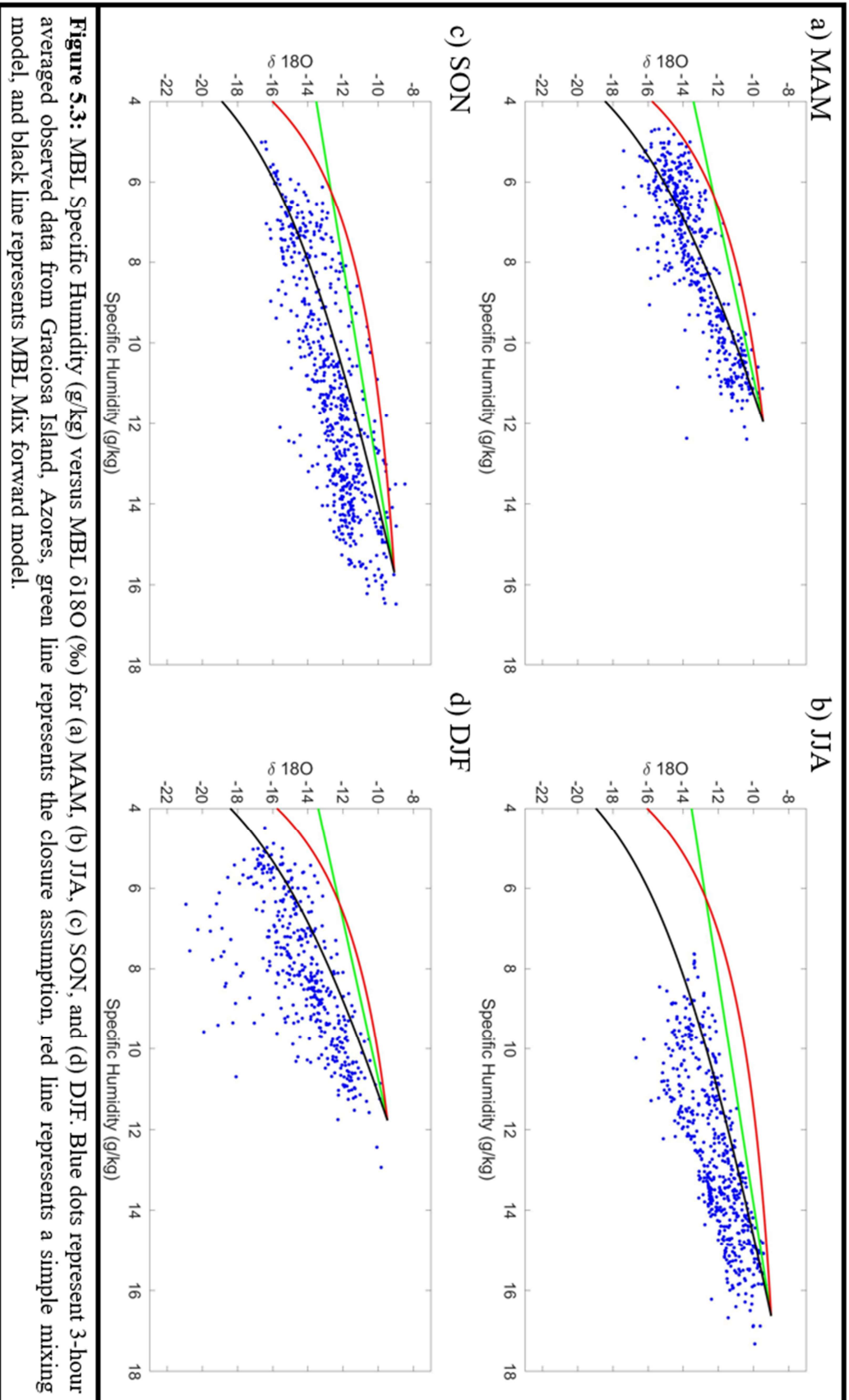
**Table 5.2:** Mean and standard deviation for SST collected using NOAA satellite data for the region surrounding Graciosa Island, Azores from March 1, 2018 until February 28, 2019. Measurements are reported for the entire time series (one year) as well as four seasons (MAM, JJA, SON, and DJF) within the one year deployment.

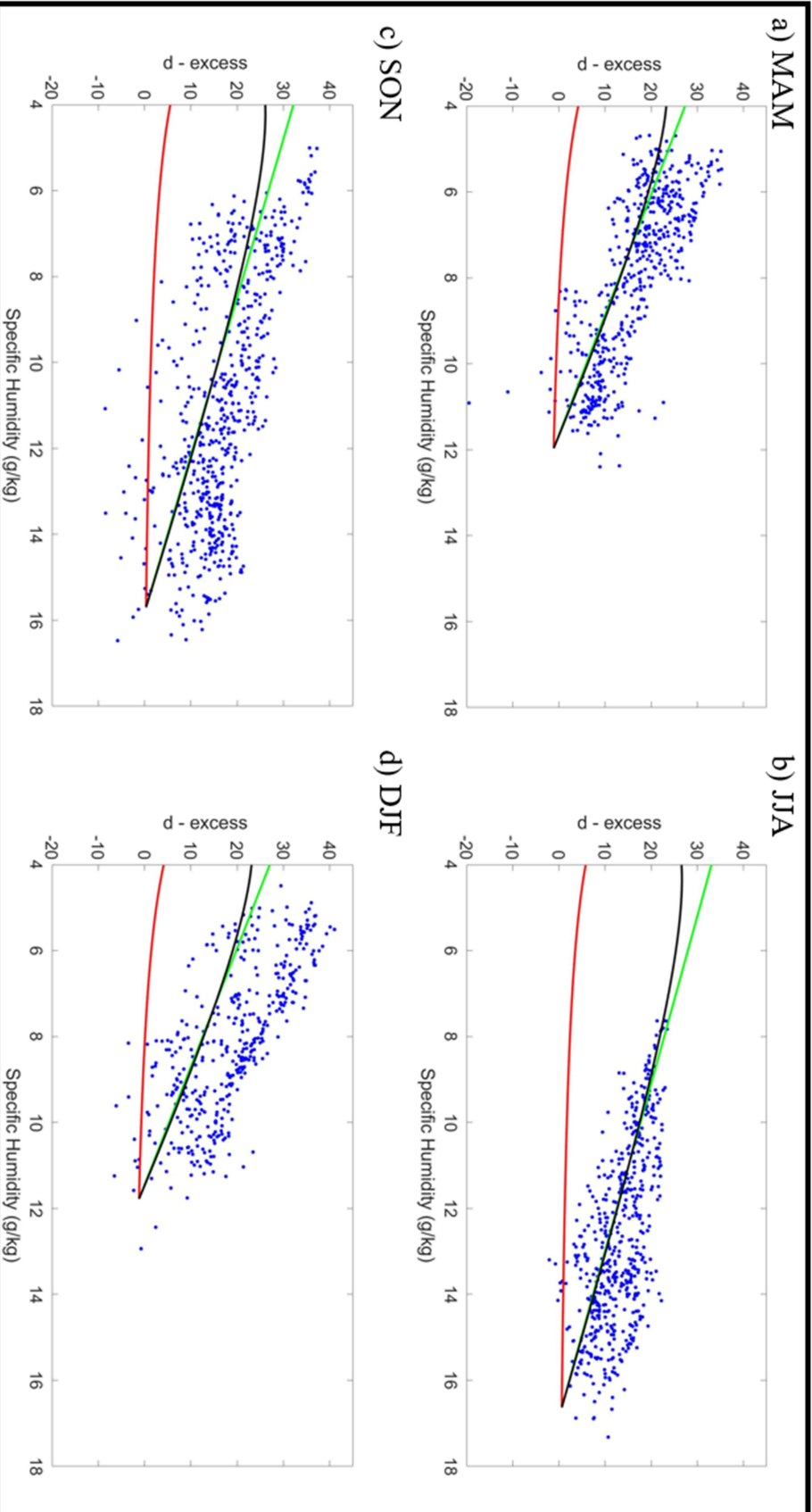
Humidity and isotope observations from each season are plotted with the closure assumption, a simple mixing model with a constant  $\delta$  of evaporative flux (Gedzelman, 1988; Galewsky and Hurley, 2010), and MBL Mix to test which model consistently best represents MBL  $\delta$  characteristics (**Figures 5.2** through **5.4**). To calculate the closure assumption line, we use humidity observations from the isotope analyzer deployed on Graciosa Island, ocean surface isotope observations from Benetti et al. (2017), seasonally averaged NOAA SST observations from the Azores region, and kinetic fractionation

factors for  $\delta D$  and  $\delta^{18}O$  from Benetti et al. (2015). To generate the simple mixing model and MBL Mix, we use output from the closure assumption and represent the LFT using midlatitude  $\delta D$ ,  $\delta^{18}O$ , and humidity climatology's developed in Benetti et al. (2018). We find the closure assumption overpredicts MBL  $\delta D$  and  $\delta^{18}O$  for every season, but generally well represents d-excess values in every season, which is consistent with the findings of Benetti et al. (2014). The simple mixing model succeeds in representing  $\delta D$ , but overestimates  $\delta^{18}O$  and underestimates d-excess. In agreement with Benetti et al. (2018), we find MBL Mix generally best represents  $\delta D$ ,  $\delta^{18}O$ , and d-excess for all seasons, reflecting the importance of considering a dynamic evaporative flux and LFT mixing in modeling the isotopic characteristics of MBL water vapor in an oceanic setting transitioning between the subtropics and midlatitudes.



**Figure 5.2:** MBL Specific Humidity (g/kg) versus MBL  $\delta D$  (‰) for (a) MAM, (b) JJA, (c) SON, and (d) DJF. Blue dots represent 3-hour averaged observed data from Graciosa Island, Azores, green line represents the closure assumption, red line represents a simple mixing model, and black line represents MBL Mix forward model.

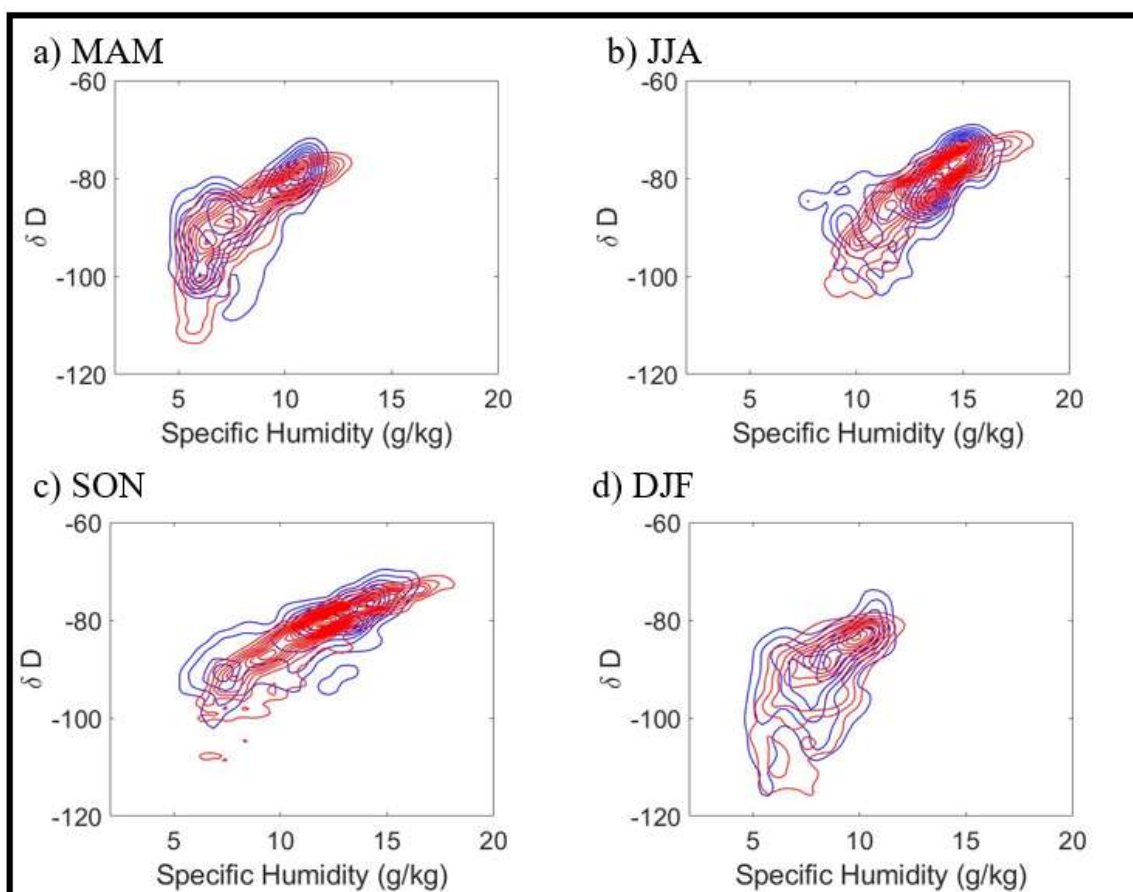




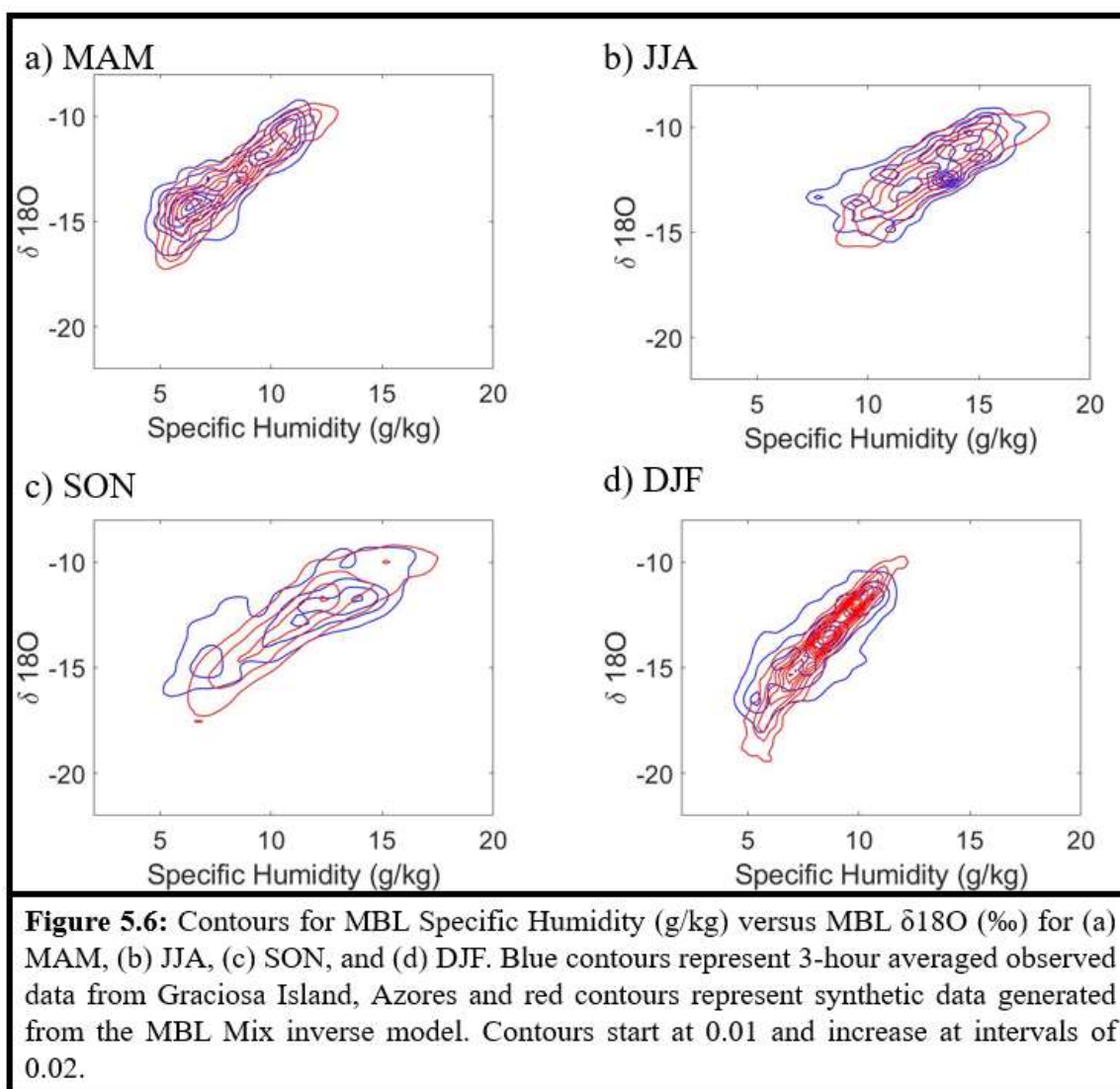
**Figure 5.4:** MBL Specific Humidity (g/kg) versus MBL d-excess (%) for (a) MAM, (b) JJA, (c) SON, and (d) DJF. Blue dots represent 3-hour averaged observed data from Graciosa Island, Azores, green line represents the closure assumption, red line represents a simple mixing model, and black line represents MBL Mix forward model.

## 5.2 MBL Mix Inverse Model Calculations

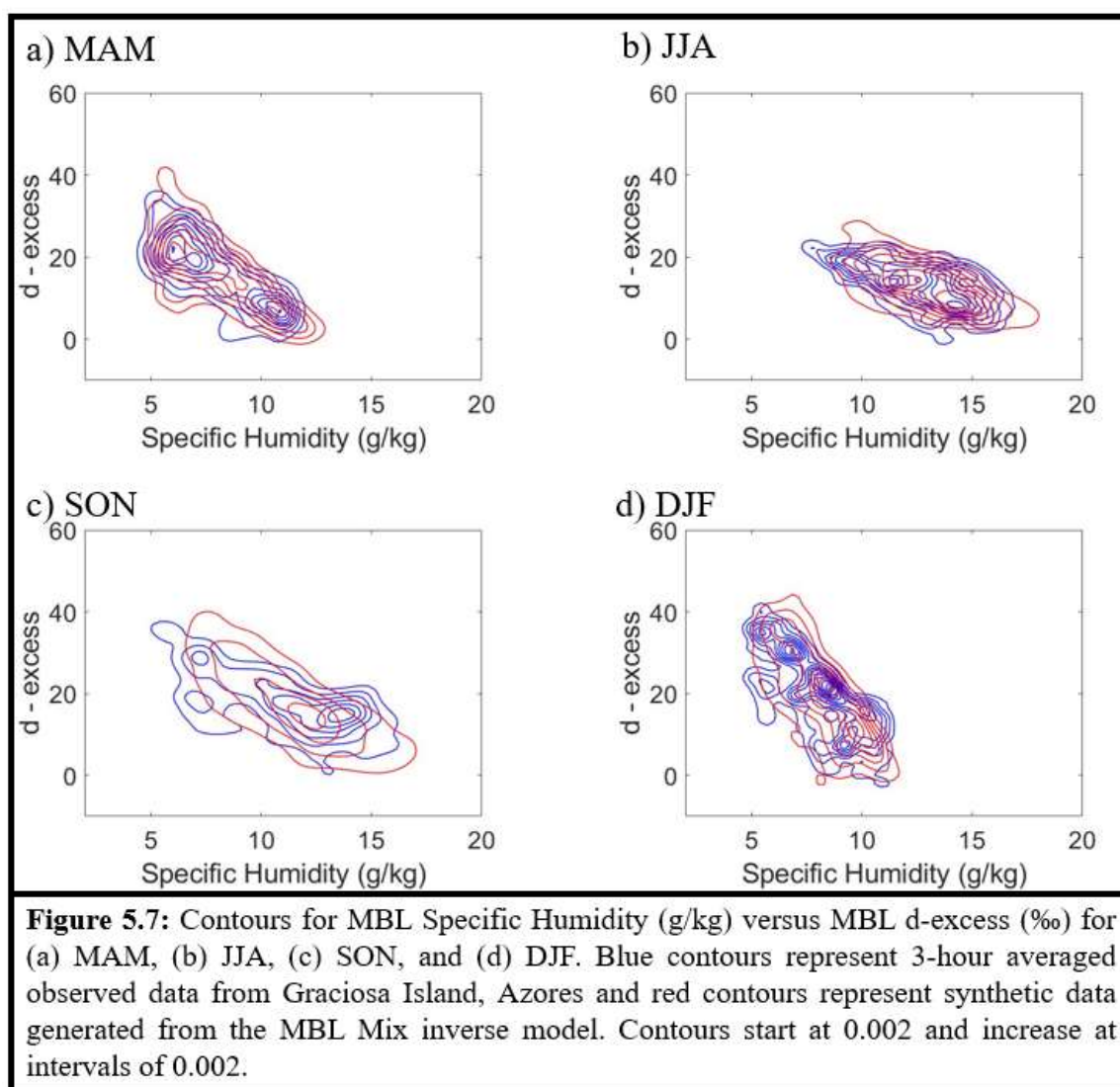
The purpose of the MBL Mix inverse model is to find an optimal solution capable of recreating observed trends in the relationship between the MBL specific humidity and  $\delta$  values in order to estimate LFT mixing. This study uses three-hour averaged data from Graciosa Island to match synthetic data to observations. In order to reduce the island's effect on observed specific humidity and  $\delta$  values, we neglect data collected when wind direction was from the southeast to southwest. This reduces the effect of using observations in the model that have recorded fractionation from the island's topography and better represents MBL conditions over the ocean. The ability of the inverse model to match observed trends is demonstrated by **Figures 5.5** through **5.7**. The goodness of fit for  $\delta D$ ,  $\delta^{18}O$ , and d-excess between synthetic and observed data is evaluated using a Kolmogorov-Smirnov test (**Table 5.3**), where a lower Kolmogorov-Smirnov test value represents a better fit.



**Figure 5.5:** Contours for MBL Specific Humidity (g/kg) versus MBL  $\delta D$  (‰) for (a) MAM, (b) JJA, (c) SON, and (d) DJF. Blue contours represent 3-hour averaged observed data from Graciosa Island, Azores and red contours represent synthetic data generated from the MBL Mix inverse model. Contours start at 0.002 and increase at intervals of 0.002.







<b>Table 5.3: Goodness of Fit Statistics for MBL Mix Inverse Model Output</b>			
<b>Season</b>	<b>K-S Statistic <math>\delta D</math></b>	<b>K-S Statistic <math>\delta 18O</math></b>	<b>K-S Statistic d-excess</b>
<b>MAM (2018)</b>	0.0882	0.0701	0.0721
<b>JJA (2018)</b>	0.0912	0.0823	0.0716
<b>SON (2018)</b>	0.0983	0.1350	0.1333
<b>DJF (2018 - 2019)</b>	0.0940	0.1060	0.0892

**Table 5.3:** Values represent the goodness of fit between the observed versus the synthetic data for specific humidity and  $\delta D$ ,  $\delta 18O$ , and d-excess, which is illustrated for each season in Figures 5.5 through 5.7 and was evaluated using a Kolmogorov-Smirnov test.

LFT mixing is defined with a beta distribution that is directly optimized by the genetic algorithm. Values from that beta distribution are then input to the inverse model to represent LFT mixing fractions. A beta distribution is bounded by  $[0, 1]$ , but the  $r$  value that represents LFT mixing in **Equation 2.2** never equals 0 unless LFT specific humidity equals 0 g/kg. The range of physically possible  $r$  values is constantly changing as the inverse model progresses, due to continued changes in the combination of the saturation specific humidity of the evaporative flux and specific humidity of the LFT used to generate MBL Mix curves within the model. Because of this quantitative relationship and because of the methods used in this study, we find  $r$  is generally required to be greater than approximately 0.3 to match observations. Estimates of LFT mixing between seasons are illustrated in **Figure 5.8**. **Table 5.4** expresses the inverse model solved alpha and beta values for the LFT mixing beta distribution as well as the mean, minimum, and maximum LFT mixing values for each season. Average LFT mixing is 0.70, 0.47, 0.53, and 0.65 for MAM, JJA, SON, DJF, respectively. Variability of mixing is highest during MAM and lowest during JJA. **Figure 5.8** additionally includes the range of monthly average low-cloud occurrence observations for each season from Rémillard et al. (2012), which are

compared to isotope-derived mixing estimates in **Section 6.4**. We additionally show the relation between isotope-derived LFT mixing and RHS in **Figure 5.9** and **Table 5.5**, which is discussed in **Section 6.6**.

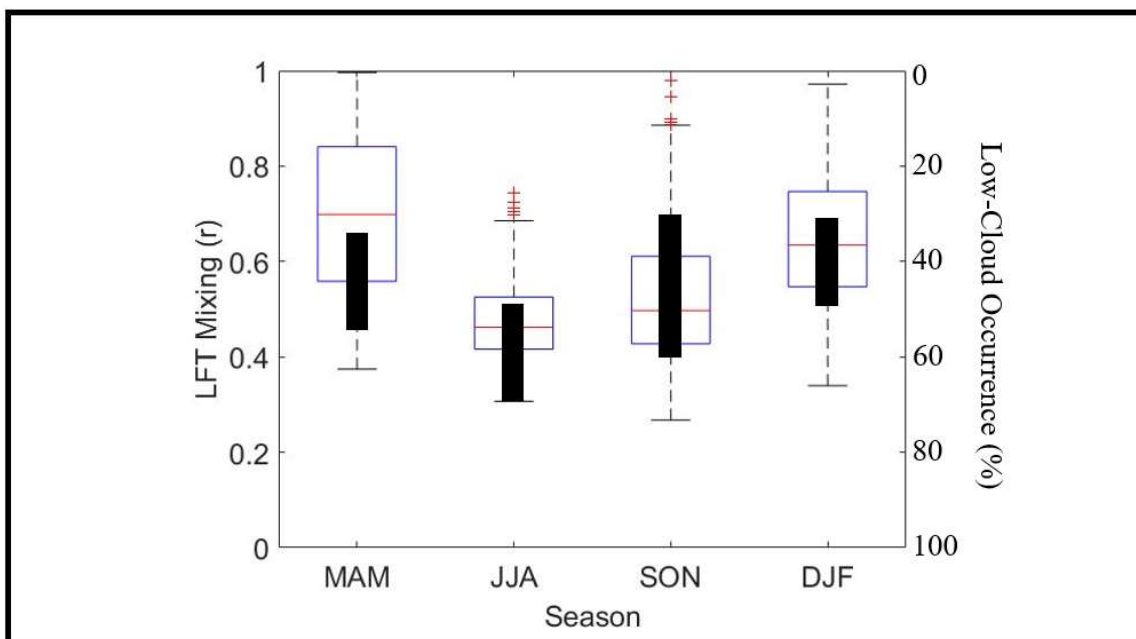


**Figure 5.8:** Box plots of MBL Mix Inverse Model solved LFT Mixing ( $r$ ) for MAM, JJA, SON, and DJF. The red line represents the median, the bottom of the box represents the 25<sup>th</sup> percentile, the top of the box represents the 75<sup>th</sup> percentile, the whiskers extend to the most extreme values, and red + symbols represent values considered outliers. Black rectangles represent the range of average low-cloud occurrence observations for each month within each season (Rémillard et al. 2012).

<b>Table 5.4: MBL Mix Inverse Model Mixing Parameter</b>					
<b>Time Period</b>	<b>LFT Mixing (fraction of mixing)</b>				
	$\alpha$	$\beta$	Mean	Min	Max
<b>MAM (2018)</b>	0.89	1.05	0.70	0.37	1.00
<b>JJA (2018)</b>	1.91	8.21	0.47	0.31	0.74
<b>SON (2018)</b>	0.98	2.74	0.53	0.27	0.98
<b>DJF (2018 - 2019)</b>	1.51	2.37	0.65	0.34	0.97

**Table 5.4:** MBL Mix inverse model solved alpha and beta parameters for LFT mixing beta distributions are reported for each season with the mean, minimum, and maximum of their distributions.

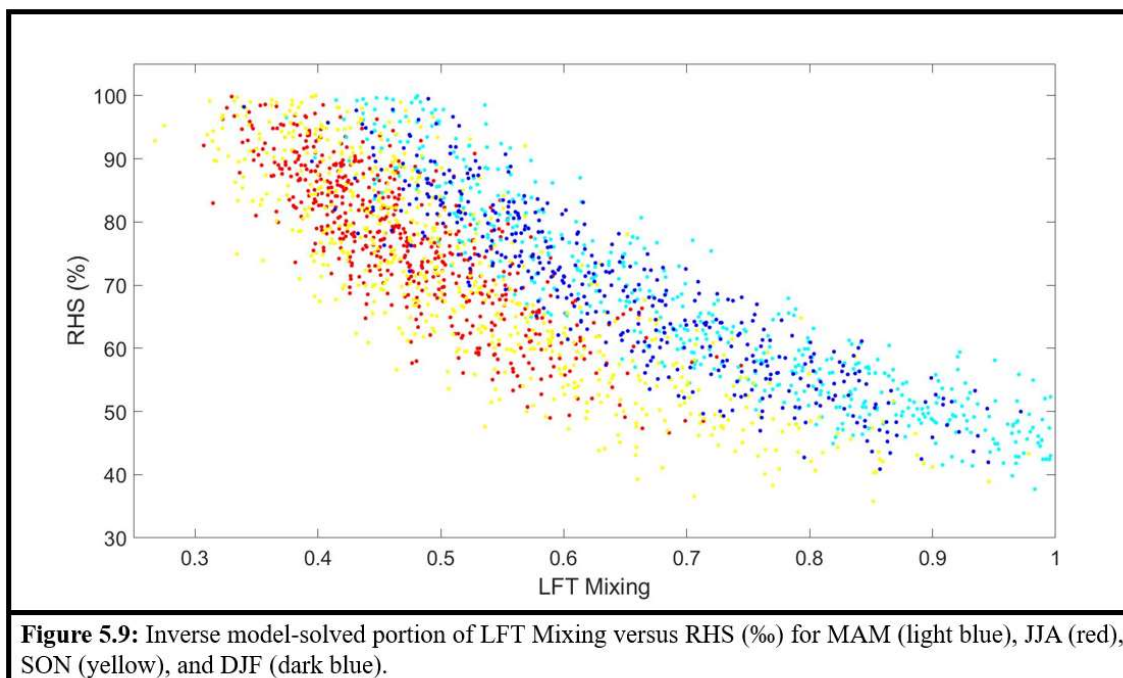


**Figure 5.9:** Inverse model-solved portion of LFT Mixing versus RHS (%) for MAM (light blue), JJA (red), SON (yellow), and DJF (dark blue).

<b>Time Period</b>	<b>R<sup>2</sup></b>	<b>2nd Degree Polynomial</b>	<b>LFT Mixing for RHS = 90%</b>	<b>LFT Mixing for RHS = 60%</b>
<b>One Year (2018 - 2019)</b>	0.68	$y = 61.7x^2 - 156x + 140$	0.38	0.71
<b>MAM (2018)</b>	0.87	$y = 108x^2 - 244x + 182$	0.48	0.75
<b>JJA (2018)</b>	0.67	$y = 91.9x^2 - 211x + 156$	0.37	0.63
<b>SON (2018)</b>	0.72	$y = 98.5x^2 - 217x + 157$	0.37	0.62
<b>DJF (2018 - 2019)</b>	0.82	$y = 75x^2 - 194x + 162$	0.45	0.73

**Table 5.5:** The strength of the correlations between LFT mixing and RHS inverse model output are shown and a second degree polynomial is generated for the entire Azores dataset as well as each season. The polynomial is used to estimate the LFT mixing from 90% and 60% RHS, and to consider how consistent the predicted LFT mixing is for different seasons.

## 6. Discussion

In this section, we compare observations from Graciosa Island to studies from the Bermuda Islands, North Atlantic Ocean tropical and subtropical cruises, and the equatorial Indian Ocean (**Section 6.1**); we explore the benefits and limitations of representing the LFT using Rayleigh fractionation (**Section 6.2**); we discuss the lower bound of LFT mixing solved by the inverse model (**Section 6.3**); we compare mixing variability and low-cloud observations between seasons (**Section 6.4**); we address the uncertainty of the MBL Mix inverse model (**Section 6.5**); and explore the added value of using water vapor isotopologue and humidity measurements to better understand mixing processes that influence low-cloud feedback compared to using humidity measurements alone (**Section 6.6**).

### 6.1 Comparison of Azores Observations to Other Study Areas

Steen Larsen et al. (2014) recorded continuous in situ isotope and humidity measurements on Bermuda between November 2011 and June 2013. They reported a time series of  $\delta^{18}\text{O}$  and d-excess for the entire study period. By comparing the two datasets we find  $\delta^{18}\text{O}$  and d-excess were more variable in the one year of measurements from Azores than the year and a half of measurements from Bermuda. In Bermuda,  $\delta^{18}\text{O}$  ranges between -8‰ and -16‰ while in the Azores it ranges between -8‰ and -21‰. d-excess ranged between -5‰ and 30‰ in Bermuda while it ranged between -20‰ and 40‰ in the Azores. This increase in variability may partly be attributed to differences in MBL specific humidity, SST, and ocean surface  $\delta$  values between the two settings, because of their effect on the isotopic composition of water vapor evaporating from a water body and mixing into

the MBL. The Azores generally experience a lower specific humidity compared to the Bermuda, which causes evaporative flux to have a more isotopically depleted  $\delta^{18}\text{O}$  and higher d-excess. The Azores region also experiences cooler SST ( $16^{\circ}\text{C}$  to  $24^{\circ}\text{C}$ ) compared to Bermuda ( $20^{\circ}\text{C}$  to  $28^{\circ}\text{C}$ ), which would cause evaporative flux from the ocean to have more isotopically enriched  $\delta^{18}\text{O}$  and lower d-excess. Ocean surface  $\delta$  values have been observed to be more isotopically depleted in the Azores region than in Bermuda (Benetti et al. 2017), which would lead to a more depleted  $\delta^{18}\text{O}$  of evaporative flux but could have variable effects on d-excess. Steen Larsen et. al (2014) also report annual averages from 2012 observations on Bermuda; the annual average of  $\delta\text{D}$  ( $-80.8\text{‰}$ ) and  $\delta^{18}\text{O}$  ( $-11.81\text{‰}$ ) were both slightly higher compared to that of the Azores ( $-87.7\text{‰}$  and  $-12.98\text{‰}$ , respectively), while average d-excess was lower in Bermuda ( $13.7\text{‰}$ ) compared to that in the Azores ( $16.1\text{‰}$ ). The Bermuda dataset additionally shows less isotopic variability of  $\delta^{18}\text{O}$  and d-excess in summer months than winter months. The Azores dataset shows the same trend in  $\delta^{18}\text{O}$  (standard deviation is  $1.40\text{‰}$  in JJA and  $2.03\text{‰}$  in DJF), but the opposite trend in d-excess (standard deviation is  $5.2\text{‰}$  in JJA and  $1.7\text{‰}$  in DJF).

Benetti et al. (2014) reported STRASSE cruise data collected between mid-August and mid-September from the subtropical North Atlantic ( $26^{\circ}\text{N}$  and  $35^{\circ}\text{W}$ ) in a region of high excess evaporation. During this survey,  $\delta^{18}\text{O}$  generally varied between  $-9.5\text{‰}$  and  $-11\text{‰}$ , but decreased by  $2.5\text{‰}$  during a precipitation event, and  $\delta\text{D}$  generally varied between  $-70\text{‰}$  and  $-80\text{‰}$ , but decreased by  $18\text{‰}$  during a precipitation event. d-excess ranged between  $5$  and  $17\text{‰}$ . During a comparable time period in the Azores, variability was generally slightly larger for  $\delta\text{D}$  ( $-74\text{‰}$  to  $-88\text{‰}$ ) and  $\delta^{18}\text{O}$  ( $-11\text{‰}$  to  $-13\text{‰}$ ). Some of this increase in isotopic variability can be attributed to a more dynamic SST during this time

period; while the STRASSE cruise observed an SST variation of less than 1°C (between 27°C and 28°C), data collected during the comparable time period in the Azores coincided with a change of approximately 2.5°C (between 23°C and 25.5°C). The STRASSE cruise area also took place in an area with more isotopically enriched ocean surface  $\delta$  values than what has been observed in the Azores region (Benetti et al. 2017). Both of these observations would lead to a more isotopically depleted and variable evaporative flux in the Azores region, which is what is observed.

Benetti et al. (2016) reported PIRATA cruise data from mid-August to mid-September that was collected in the tropical Atlantic Ocean between 6°S and 6°N. This study reports a time series of observed  $\delta^{18}\text{O}$  and d-excess from the study period. Observations show  $\delta^{18}\text{O}$  generally stayed between -10‰ and -12‰ during the study period but ranged between -10‰ and -18‰. d-excess ranged between 6‰ and 16‰. During the cruise, SST ranged between 27°C and 29.5°C. Data from the Azores for a comparable time period has a similar range but slightly more isotopically depleted  $\delta^{18}\text{O}$  (-11‰ to -13‰), a higher and more variable d-excess range (10‰ to 23‰), and the same variability in SST but a cooler SST (23°C to 25.5°C).

Kurita et al. (2011) reported cruise data from October to December 2006 that was collected in the tropical Indian Ocean. This study reports a time series of observed  $\delta\text{D}$  and d-excess from the study period that is divided between convectively inactive and convectively active times. Convectively inactive times correspond to measurements of  $\delta\text{D}$  generally between -70‰ and -120‰, but convectively active times expand this range to between -70‰ and -170‰. Convectively inactive times correspond to d-excess measured generally between 12‰ and 21‰, but convectively active times expand this range to

between 7‰ and 23‰. In the Azores dataset, we do not separate convectively active from convectively inactive measurements. The  $\delta D$  observations from the Azores (-70‰ to -130‰) have greater variability than the Indian Oceans convectively inactive time, but less variability than the convectively active period. The d-excess observations in the Azores (-8‰ to 37‰) have greater variability than both the convectively active and inactive periods of time.

## 6.2 Benefits and Limitations of Rayleigh Fractionation

Many studies do not have available instrumentation to simultaneously record isotope observations in multiple locations. Some studies overcome this limitation by using isotope data collected using satellite instrumentation (Worden et al., 2012). However, satellite data is restricted spatially, temporally, and by uncertainty constraints. Because of this, we attempt to use Rayleigh fractionation to constrain LFT characteristics using tools that were available to us at the DOE ARM facility and would commonly be available to other studies at a wide variety of locations. Setting up Rayleigh fractionation only requires MBL  $\delta$  observations and a temperature profile from local weather balloon soundings. MBL  $\delta$  values allow us to constrain the likely range of initial  $\delta$  values that would undergo Rayleigh Fractionation. The temperature profile is used to calculate a profile of temperature-dependent equilibrium fractionation factors that would progressively influence the initial  $\delta$  values.

Benetti et al. (2018) used spaceborne instruments, including Tropospheric Emission Spectrometer (TES, Worden et al., 2012) and Infrared Atmospheric Sounding Interferometer (Lacour et al., 2012), to construct climatology profiles for specific humidity and  $\delta D$  to constrain the LFT used for the MBL Mix forward model. They calculated  $\delta^{18}O$



by using the  $\delta D$  from 3.5 km height and assumed d-excess of 15 or 30‰. By using Rayleigh fractionation, this study advances past previous work in two ways. (1) We do not need to calculate  $\delta^{18}O$  using an assumed d-excess. Instead, we can calculate the progressive effects of fractionation on both  $\delta D$  and  $\delta^{18}O$  individually in order to build profiles of  $\delta D$ ,  $\delta^{18}O$ , and specific humidity for a large portion of the troposphere. (2) Instead of picking the height at which we suspect LFT air mixing into the MBL to be sourced, we can allow the inverse model to solve for this parameter. By building a tropospheric profile of these characteristics, we can allow the inverse model to pick a dry end-member point that represents the best-fit  $\delta D$ ,  $\delta^{18}O$ , and specific humidity combination that will allow LFT mixing to match MBL observations while using physically constrained values to do this.

A limitation of this approach is that the Rayleigh model of isotopic depletion is an idealized model and LFT observations do not always lie along a Rayleigh curve (Yoshimura et al., 2008). A Rayleigh curve can be considered a reference point and deviation from Rayleigh can be due to a number of factors, one of which is mixing between air masses (Galewsky and Hurley, 2010). Mixing results in the LFT  $\delta$  being isotopically more enriched than what is predicted by Rayleigh. This study considered addressing this limitation by using a simple mass balance mixing model (Galewsky and Hurley, 2010) to generate a mixing curve between two points along a Rayleigh curve and to represent the LFT with a point along this secondary curve rather than the Rayleigh curve. We decided against this approach for two reasons. (1) The mixing curve can be highly variable based on the two points along a Rayleigh curve chosen to generate the mixing curve. This would lead to poorly constrained LFT characteristics. (2) The computing power required for the MBL Mix inverse model to iteratively calculate an additional mixing curve from two points

along each Rayleigh curve would result in an inefficient model, especially considering it would lead to a more poorly constrained LFT. This study seeks the simplest model set-up capable of reproducing observed MBL trends, and **Figures 5.5** through **5.7** show that the LFT characteristics chosen from a Rayleigh curve can meet this goal.

An additional source of deviation from a Rayleigh Curve is due to cloud condensate re-evaporation (Noone, 2012). This leads to observed  $\delta$  values falling below the Rayleigh curve. The annual range of precipitation experienced by the Azores is generally between 20 and 40% occurrence. However, it often completely evaporates prior to reaching the surface. Intense precipitation is more common in the fall and winter than the other seasons, due to frequent crossings of the North Atlantic storm track (Rémillard et al., 2012). Thus, deviation from Rayleigh due to re-evaporation is more common during these seasons. Benetti et al. (2015 and 2018) explain that the MBL Mix forward model does not simulate conditions where rain re-evaporation influences  $\delta$ . This limitation of the MBL Mix forward model carries over into the MBL Mix inverse model. Because the MBL Mix inverse model does not consider these conditions, we do not consider deviation from Rayleigh due to rain re-evaporation to add any additional limitation to the model when representing the dry endmember of this model.

### **6.3 LFT Mixing Lower Bound**

As defined by **Equation 2.2**, LFT mixing never equals 0. This study finds LFT mixing is generally calculated to be greater than 0.3, meaning a minimum of 30% LFT moisture mixing into the MBL is required to match humidity and  $\delta$  observations from the Azores in this analysis. In Benetti et al. (2018), data from the subtropics and midlatitudes is plotted with three MBL mix forward model curves that were each generated using

observed conditions those measurements were recorded during. We can roughly estimate the minimum  $r$  from Benetti et al. (2018) by dividing the LFT specific humidity used to generate the MBL mix curve intersecting the data by the specific humidity of the most humid observation from each dataset. By doing so, we find the minimum  $r$  values to be approximately 0.17 and 0.13 for the two midlatitude datasets and approximately 0.12 for the subtropical dataset. One reason the minimum  $r$  value in our analysis is determined to be higher than Benetti et al. (2018) is due differences in how these two studies have constrained properties of the LFT. While Benetti et al. (2018) constrain the LFT using TES data, this study uses Rayleigh fractionation. By definition, Rayleigh fractionation exclusively occurs when humidity is at saturation, meaning the specific humidity of the LFT used in this study is at saturation (between 5.3 and 5.9 g/kg), making it higher than the previous MBL mix study (between 1.7 and 2.14 g/kg) and our minimum  $r$  value is higher. If we were to plot observations from the Azores with an MBL mix curve generated using the subtropical (or midlatitudes) LFT characteristics used in Benetti et al. (2018), our minimum  $r$  values would roughly be 0.17 (0.14), 0.12 (0.10), 0.13 (0.10), and 0.17 (0.13) for MAM, JJA, SON, and DJF, respectively. Although a consequence of using Rayleigh fractionation is a higher minimum  $r$ , we argue that this method does not add any limitation to the ability of the inverse model to estimate seasonal-scale trends in mixing that match observed data.

#### **6.4 Seasonal-Scale LFT Mixing Variability and Low-Clouds**

Inverse model-derived mixing estimates of four seasons in the Azores are reported on **Table 5.4** and illustrated on **Figure 5.8**, where they are compared to the range of average low-cloud occurrence observations from a 19-month long field campaign at the DOE ARM

facility on Graciosa Island published by Rémillard et al. (2012). Rémillard et al. (2012) reported clouds occurred frequently over Graciosa Island, with a maximum occurrence of 80% during the winter and spring months and a minimum of 60 to 65% during the summer months. This pattern of cloud occurrence for all cloud types anticorrelated with the seasonal cycle of low-clouds, which are the dominant cloud type in the region, observed throughout all seasons, and reach their maximum during the summer and fall seasons during the build-up of the Azores anticyclone. The build-up of this high-pressure system is strongest in the summertime and promotes low-cloud formation through a stronger and less variable inversion that caps the MBL. MBL Mix inverse model calculates the lowest seasonal mixing averages for JJA (0.47) and SON (0.53). JJA had the lowest mixing variability of all seasons (variance of 0.006) while SON had moderate variability (0.018). Rémillard et al. (2012) reported monthly averages for low-cloud occurrence which ranged between 50 through 70% for JJA and 30 through 60% for SON. The inverse model calculated the highest seasonal mixing averages for MAM (0.70) and DJF (0.65). MAM had the highest mixing variability (0.027) and DJF had moderate variability (0.017). The monthly average low-cloud occurrence reported by Rémillard et al. (2012) ranged between 35 to 55% for MAM and 30 through 50% for DJF. This shows that the MBL Mix inverse model is capable of using isotope and humidity observations to estimate mixing trends that are consistent with observations of low-cloud formation.

### **6.5 Uncertainty of MBL Mix Inverse Model**

The K-S statistic used to determine the optimized MBL Mix inverse model output is reported on **Table 5.3** for each season. Using a K-S statistic to evaluate error also returns a p value that is examined against a significance level ( $\alpha = 0.1$ ) to test the null

hypothesis that the synthetic data and observed data are generated with the same distribution. If the two datasets are determined to fall along the same distribution ( $p > \alpha$ ), then the model returns an H-value of 0, but if the two datasets are determined to fall along different distributions ( $p < \alpha$ ), then the model returns an H-value of 1.

The H-values for specific humidity versus  $\delta D$ ,  $\delta^{18}O$ , and d-excess were determined to be 0 for each season in this study, with the exception of  $\delta^{18}O$  and d-excess for SON. There are several potential contributing factors to this. (1) SON is the season with the largest number of observational points. Having a larger observational dataset makes matching it with synthetic data that has a H-value of 0 less likely because it is more difficult to get a higher p value. This means that even though the two distributions may visually appear indistinguishable, the model will still determine an H-value of 1. (2) The atmospheric processes occurring during this season may be too variable and also deviate from what can be represented by MBL Mix. The high-pressure system that peaks in the summer also persists into September, but then lessens as the area starts to be crossed by the North Atlantic storm track in the fall. The stability of the anticyclone and the convective activity associated with storms represent very different atmospheric conditions that may produce a distribution of observed data points difficult to match with the beta distributions used in the inverse model. The storms also represent unstable conditions where rain re-evaporation would influence the water vapor  $\delta$  values, so they deviate from the stable conditions MBL Mix is designed to represent. Although this H-value criteria can be used to determine the significance of the fit between datasets, we argue the synthetic  $\delta^{18}O$  and d-excess for SON do not deviate from the observed  $\delta^{18}O$  and d-excess in a visually noticeable way (**Figures 5.6 and 5.7**) compared to the other seasons that do have an H-

value of 0. Because of the synthetic data still broadly overlaps the area covered by the observed data, the SON season should still be considered for studying seasonal mixing trends.

Future work for this study may include the uncertainty analysis approach completed by Galewsky (2018), where a 95% confidence interval is generated for each of the model parameters. This is done by running MBL Mix inverse model many (a minimum of 100) times using bootstrapping techniques with resampling and substitution. This level of uncertainty analysis is out of the scope of this thesis due to limitations of the computing power required to perform this level of analysis using the MBL Mix inverse model. We note Galewsky and Rabanus (2016) also did not include this uncertainty analysis in their study using inverse modeling. Instead of bootstrapping, we compare the output from the pool of different inverse model runs used to determine the best-fit model set-up by adjusting both the population size of each generation of the genetic algorithm (using population sizes of 2000 and 3000) as well as the upper bound of the alpha and beta values used to generate the beta distribution of each parameter optimized by the genetic algorithm (using alpha and beta value upper bounds of 25, 50, and 100).

The variability in LFT mixing found between different model set-ups is recorded on **Table 6.1**. Average LFT mixing ranges between 0.59 and 0.73 for MAM, 0.46 and 0.50 for JJA, 0.46 and 0.57 for SON, and 0.42 and 0.66 for DJF. We note that the DJF model set-ups with the lowest average LFT mixing also have the highest average K-S statistics ( $> 0.05$  higher than other DJF model set-up average K-S statistics). If the two DJF model set-ups with the particularly high K-S statistics were left out of consideration, the range of average LFT mixing would be 0.52 to 0.66. We argue this approach to uncertainty analysis

supports the ability of inverse modeling, using a combination of genetic algorithm optimization, MBL Mix, and Rayleigh fractionation, to reproduce observed trends in isotope and humidity data and provide a constrained estimation of LFT mixing.

Table 6.1: MBL Mix Inverse Model Mixing Variability						
Model Set-Up		MAM (2018) LFT Mixing (fraction of mixing)				
		$\alpha$	$\beta$	Mean	Min	Max
Population 2000	Upper Bound 25	0.89	1.05	0.70	0.37	1.00
	Upper Bound 50	1.03	1.34	0.68	0.37	1.00
	Upper Bound 100	1.24	2.20	0.59	0.32	0.99
Population 3000	Upper Bound 25	0.99	0.92	0.73	0.38	1.00
	Upper Bound 50	0.90	1.02	0.71	0.40	1.00
	Upper Bound 100	1.11	1.72	0.64	0.38	0.98
Model Set-Up		JJA (2018) LFT Mixing (fraction of mixing)				
		$\alpha$	$\beta$	Mean	Min	Max
Population 2000	Upper Bound 25	1.91	8.21	0.47	0.31	0.74
	Upper Bound 50	2.08	8.84	0.47	0.31	0.80
	Upper Bound 100	1.58	6.57	0.48	0.31	0.74
Population 3000	Upper Bound 25	1.67	6.90	0.48	0.31	0.77
	Upper Bound 50	1.99	9.00	0.46	0.30	0.76
	Upper Bound 100	1.83	7.22	0.50	0.34	0.75
Model Set-Up		SON (2018) LFT Mixing (fraction of mixing)				
		$\alpha$	$\beta$	Mean	Min	Max
Population 2000	Upper Bound 25	1.18	3.51	0.51	0.27	0.92
	Upper Bound 50	1.09	2.33	0.57	0.31	0.98
	Upper Bound 100	1.14	3.95	0.46	0.24	0.87
Population 3000	Upper Bound 25	0.98	2.74	0.53	0.27	0.98
	Upper Bound 50	1.27	4.13	0.49	0.26	0.98
	Upper Bound 100	1.02	2.38	0.55	0.30	0.98
Model Set-Up		DJF (2018-2019) LFT Mixing (fraction of mixing)				
		$\alpha$	$\beta$	Mean	Min	Max
Population 2000	Upper Bound 25	2.00	3.47	0.63	0.32	0.94
	Upper Bound 50	2.30	6.32	0.52	0.31	0.82
	Upper Bound 100	1.70	6.57	0.43	0.28	0.78
Population 3000	Upper Bound 25	1.51	2.37	0.65	0.34	0.97
	Upper Bound 50	1.48	2.34	0.66	0.40	0.96
	Upper Bound 100	2.00	8.21	0.42	0.30	0.74

**Table 6.1:** Summary of LFT Mixing results for different MBL Mix inverse model set-ups that were tested to find an optimal solution (a solution with the lowest possible K-S statistic) by changing the genetic algorithm's population for each generation (either a population of 2000 or 3000 individuals) and the upper bound of the alpha and beta parameter used to generate the beta distributions for each parameter optimized by the inverse model (upper bounds of 25, 50, and 100).



## 6.6 Advantage of Using Water Vapor Isotopologues in Addition to Humidity

Previous work has argued water vapor isotopologues do not provide additional constraints on atmospheric processes that are already possible using humidity measurements alone. Duan et al. (2018) used a single column model to show free tropospheric  $\delta D$  is insensitive to convective parameters and variations in  $\delta D$  are comparable or smaller than uncertainty to conclude  $\delta D$  is unlikely to provide information about cloud forming processes that cannot be learned exclusively from RH. Although their work highlights the importance of considering the crossroads of water vapor isotopologue sensitivities and uncertainties in climate models, the study design uses highly uncertain convective parameters to estimate changes in water vapor isotopologues that already have high uncertainties due to combining remote sensing uncertainties with model assumption uncertainties (the study did not consider a dynamic temperature-dependent equilibrium fractionation factor and did not allow changes in the MBL water vapor isotopologue composition), so their conclusion is not surprising.

RH has been given particularly high importance in climate modeling studies to better understand changes to the water cycle under future warming climate conditions, specifically with regards to cloud feedback (Sherwood et al., 2010; Rieck et al., 2012; Sherwood et al., 2014; Duan et al., 2018). We consider if there is a quantitative relation between isotope-derived LFT mixing and RHS to explore if the dependent variable RHS can be used to approximate the independent variable LFT mixing. Note that we use RHS rather than RH in this consideration, because the MBL Mix inverse model outputs RHS rather than RH, so RH is considered as a function of SST rather than ambient air temperature. **Figure 5.9** illustrates this relation. While there is a general correlation among

the entire dataset ( $R^2$  is 0.68), MAM and DJF have the highest correlation between the two variables ( $R^2$  of 0.87 and 0.82, respectively) and fall along similar curves, while JJA and SON have a slightly lower correlation ( $R^2$  of 0.67 and 0.72, respectively) and fall along similar curves. We point out that it is interesting the correlation is lowest for JJA, the season with the highest occurrence of low-clouds and most similar atmospheric conditions to the subtropics, where low-cloud feedback is of exceptional interest in climate models.

The relation between isotope-derived LFT mixing and RHS does not appear to be linear, particularly at higher LFT mixing values and lower RHS values, so we fit the entire dataset as well as each individual season with a 2<sup>nd</sup> degree polynomial to explore if RHS can be used to estimate LFT Mixing (**Table 5.5**). If an RHS of 90% is used to estimate LFT mixing, MAM and DJF predict an LFT mixing of approximately 0.48 and 0.45, respectively, while both JJA and SON predict an LFT mixing of approximately 0.37. If an RHS of 60% is used to estimate LFT mixing, MAM and DJF predict an LFT mixing of approximately 0.75 and 0.73, respectively, while JJA and SON predict an LFT mixing of approximately 0.63 and 0.62, respectively. When using the entire dataset to predict LFT mixing, a higher RHS predicts values closer to those estimated by JJA and SON (0.38 LFT mixing for 90% RHS) and a lower RHS predicts values closer to those estimated by MAM and DJF (0.71 LFT mixing for 60% RHS). Although there is certainly a strong relation between LFT mixing and RHS, **Figure 5.9** and **Table 5.5** support this quantitative relation to be dynamic between seasons in the Azores, meaning RHS alone is not a consistent predictor of a unique LFT mixing value.

A possible argument from those who do not support the use of water vapor isotopologues in atmospheric studies against the above described relation between LFT

mixing and RHS is that all values used to explore this quantitative relation are isotope-derived (RHS and LFT mixing are both MBL Mix inverse model output) and that we use RHS instead of RH. We address this concern with the following observation and discussion. If we were to approach estimating seasonal trends of LFT mixing in the Azores without isotopes and instead based on changes in observed RH from the DOE ARM met station, we would conclude mixing, and thus low-cloud occurrence, is the same between JJA (RH mean is 76% and standard deviation is 10.8%) and DJF (RH mean is 78% and standard deviation is 10.7%) because the distribution of observed RH is essentially the same. Based on observations from Rémillard et al. (2012), this trend in the RH and low-cloud relation does not match observations, where the season with the highest occurrence of low-clouds is JJA and the lowest occurrence of low-clouds is DJF. The isotope-derived LFT mixing estimates provide us with a more integrated story. Water vapor isotopologues record environmental factors not always as sensitively recorded by RH that influence low-clouds (for example, inversion strength). This allows them to provide LFT mixing estimates that are consistent with the relation between large- and small-scale mixing and low-cloud feedback that has been shown to be the greatest source of uncertainty in climate modeling (Sherwood et al. 2014).

The results of our study using the MBL Mix inverse model support an added value from combining humidity measurements with water vapor isotopologues. In contrast to Duan et al. (2018), by using in situ measurements of humidity and water vapor isotopologues that have a significantly lower uncertainty than those collected via remote sensing, we are able to provide a more constrained LFT mixing estimate. The MBL Mix inverse model has particular added value because it allows us to consider not only the

quantity of water vapor in the air, but also the sources of that water vapor. By using a measurement that is sensitive to a wide variety of processes that may influence mixing, relative humidity, and cloudiness, such as changes in SST, inversion strength, and MBL height, further studying water vapor isotopologues can potentially clarify ambiguous results from previous work that has failed to determine the sign and extent of low-cloud feedback.

This study does not advocate that water vapor isotopologues are an immediate solution for low-cloud feedback in climate models. Stable isotope measurements of water vapor are sensitive recorders of many processes in the atmospheric hydrologic cycle and quantitatively constraining each of those processes is very difficult (Risi et al. 2019). However, this study has demonstrated a quantitative relation between water vapor isotopologues and LFT mixing that is not recorded by humidity measurements alone and should be further explored as a potential measurement tool to improve understanding of the quantitative relation between isotope-derived mixing and low-cloud feedback. This can be done by applying isotope-derived mixing values from in situ measurements to isotope-enabled single column models. By doing so, the sensitivity of GCMs to different parameterizations of low-cloud feedback can be tested and results will provide a quality check on the methods used to represent low-cloud feedback in climate models, thereby informing improved simulation.

## 7. Conclusions

In this study, we present a new dataset that includes one year of humidity and water vapor isotopologue measurements recorded at the DOE ARM facility on Graciosa Island, Azores. These observations are compared to data collected at tropical and subtropical regions in the Atlantic and Indian Oceans to show that the Azores observations have higher variability in  $d$ -excess than the other locations as well as equal or higher variability in  $\delta$  values than the other locations except for the Indian Ocean. Observations from the Azores are also compared to three models, including the closure assumption, a simple mixing model (Gedzelman, 1988), and a mixing model that accounts for a dynamic evaporative flux (MBL Mix; Benetti et al. 2018), to show mixing from the LFT and a dynamic evaporative flux are required to consistently match observed MBL  $\delta$  values.

The primary goal of this study was to explore the ability of water vapor isotopologues to record LFT mixing, due to its important implications on low-cloud feedback and its associated uncertainty in climate models. We do this by using the MBL Mix forward model to build an inverse model (MBL Mix inverse model) capable of using isotope and humidity observations from the MBL to estimate LFT mixing. Many studies are limited by their inability to measure the LFT directly, and this study shows that this limitation can be overcome by using a Rayleigh model of isotopic depletion to represent LFT characteristics. We use observations from the Azores with the MBL Mix inverse model to estimate seasonal-scale LFT mixing average and variability for MAM 2018, JJA 2018, SON 2018, and DJF 2018 to 2019.

The results of this study show synthetic data generated by the MBL Mix inverse model can reproduce observed isotope and humidity trends in the Azores. Under the current inverse model setup, LFT mixing is generally required to be greater than 0.3 to match observed trends. When we compare LFT mixing estimates to previous work completed in the Azores by Rémillard et al. (2012), we find LFT mixing is calculated to be lowest (highest) during the seasons that historically are recorded with the highest (lowest) low-cloud occurrence. Although this study does not quantify the extent to which changes in isotope-derived LFT mixing correspond to changes in low-cloud occurrence, we show water vapor isotopologues have successfully estimated trends in LFT mixing associated with expected changes in low-cloud cover (where more mixing leads to less low-cloud cover, as demonstrated by Sherwood et al., 2014) and provide an inverse modeling tool by which future work can investigate the quantitative relation. We show isotope-derived RHS and LFT mixing are clearly related, but this relation is not consistent between all seasons and leads to a broad range of LFT mixing estimates for a given RHS. Additionally, trends in the distribution of seasonal observations of RH in the Azores do not indicate the same trends in LFT mixing, and that these trends would predict LFT mixing that is inconsistent with observations of low-cloud cover. This study concludes water vapor isotopologues provide unique information about the mixing processes that will determine future low-cloud feedback, and that this information cannot be gained with humidity measurements alone in this study setting. Water vapor isotopologue measurements should therefore be further pursued as a potential method to improve our understanding of LFT mixing and low-cloud cover. By doing so, they may provide useful knowledge regarding low-cloud

feedback that leads to more realistic climate model simulations and more constrained estimates of likely future temperature conditions.

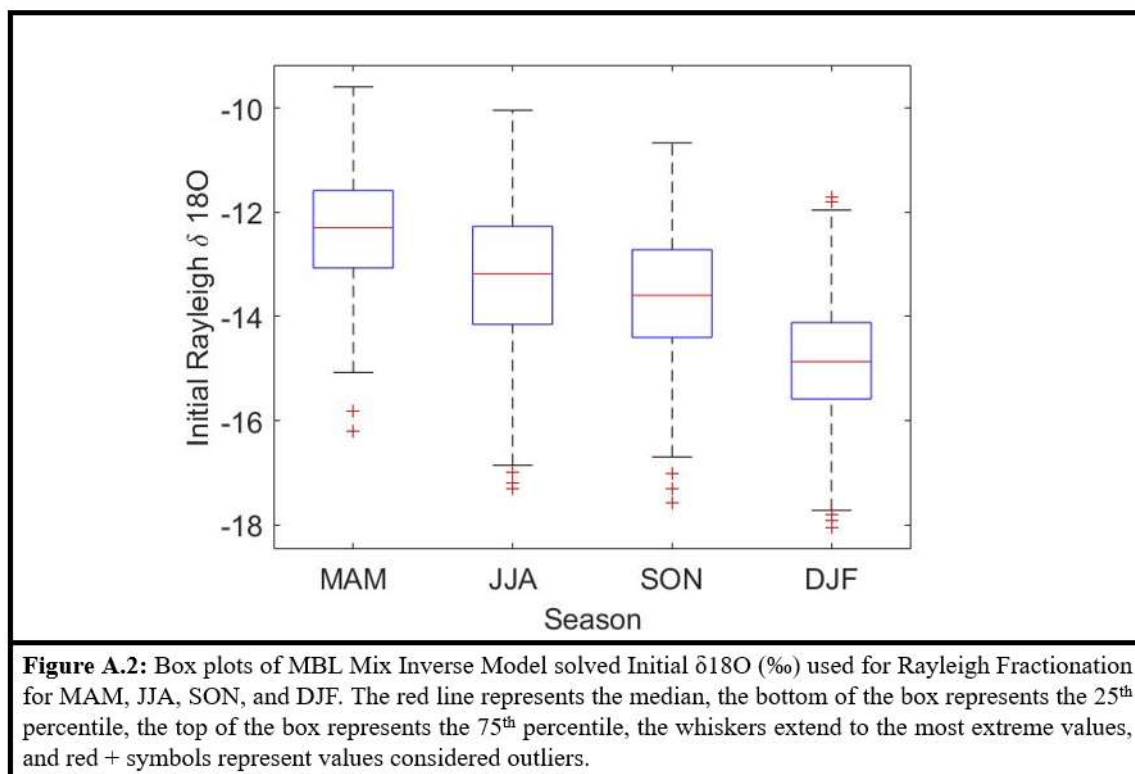
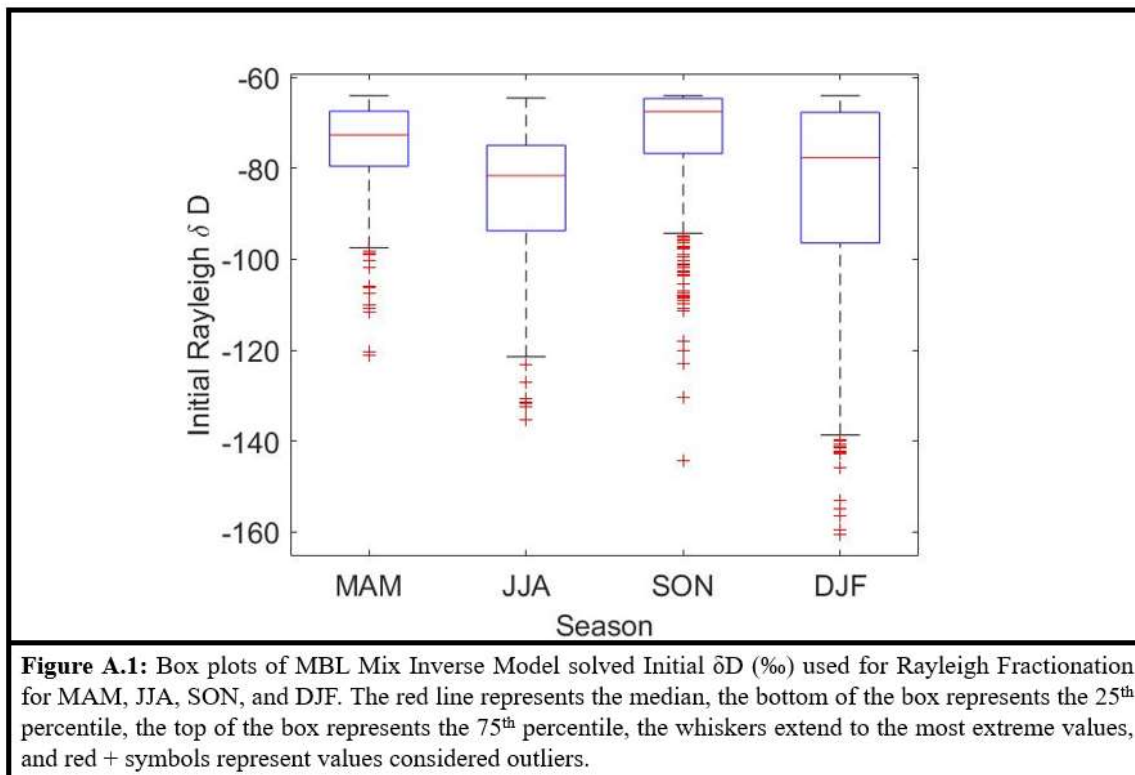
**Appendix:**

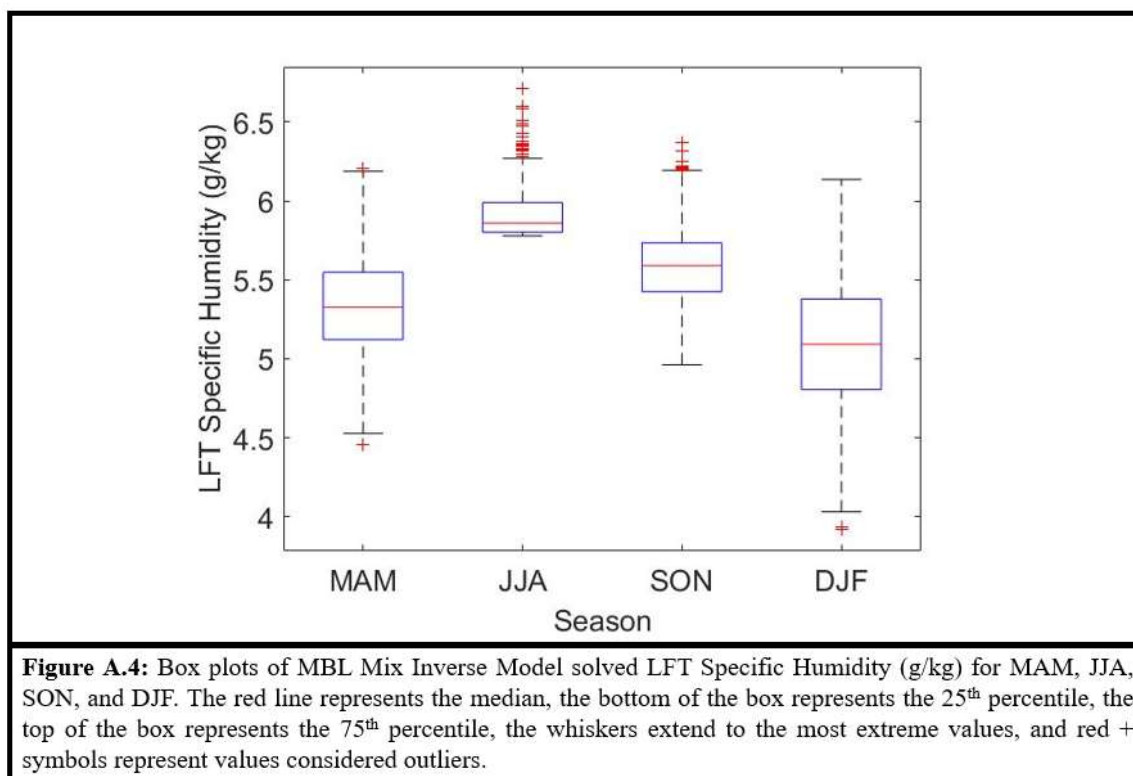
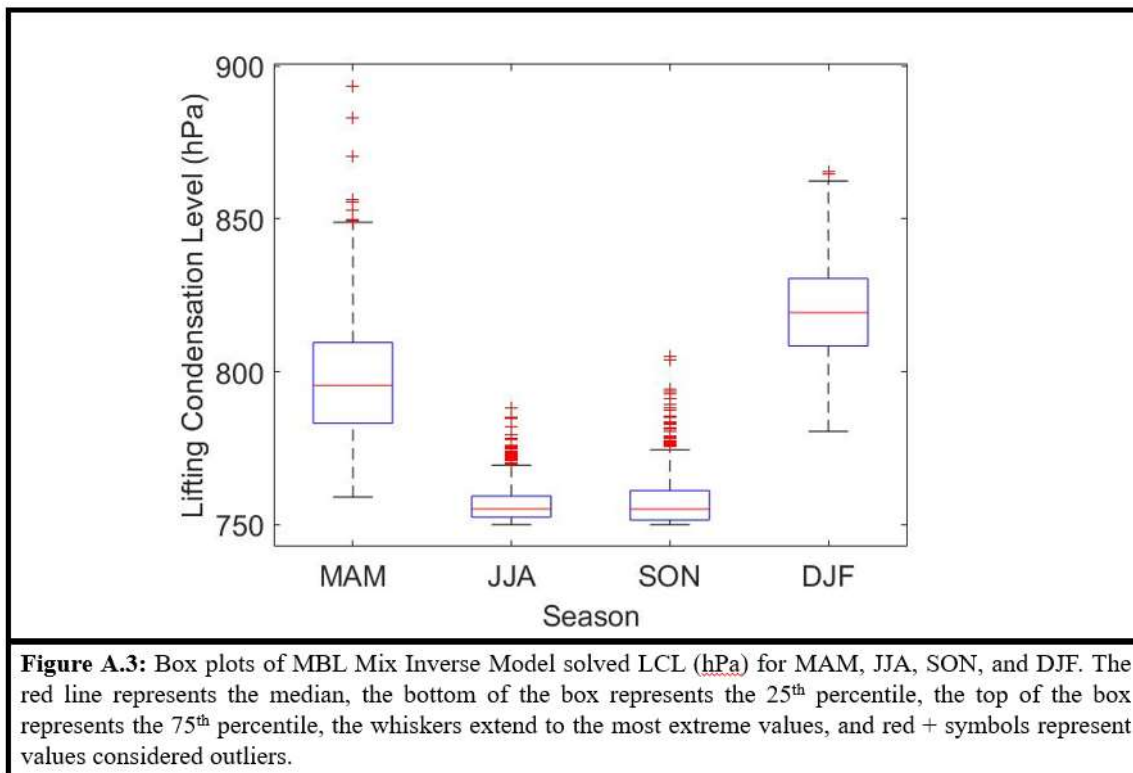
**Table A.1** documents the parameters of the MBL Mix inverse model. This includes variables directly optimized by the MBL Mix inverse model's genetic algorithm, variables indirectly optimized within the inverse model, or variables used within the model that were generated using observational data for each season. Parameters directly optimized by the inverse model's genetic algorithm are those that the genetic algorithm continually adjusts within an upper and lower bound to solve for an optimal solution capable of reproducing observed trends. This includes beta distribution used to generate values for initial  $\delta D$  and  $\delta^{18}O$  values used for Rayleigh fractionation, lifting condensation level used to begin Rayleigh fractionation, LFT specific humidity,  $\delta D$  and  $\delta^{18}O$  of the ocean surface, and LFT mixing. Parameters of the MBL Mix inverse model that were indirectly optimized by the genetic algorithm include LFT  $\delta D$  and  $\delta^{18}O$  as well as MBL specific humidity,  $\delta D$ , and  $\delta^{18}O$ . Indirectly optimized by the genetic algorithm means these variables were calculated through their numerical relation to the other parameters that were directly optimized. Evaporative flux saturation specific humidity was not optimized directly or indirectly, but rather calculated by using observational data of surface pressure and NOAA SST measurements. Parameters are illustrated in **Figures A.1** through **A.12**.

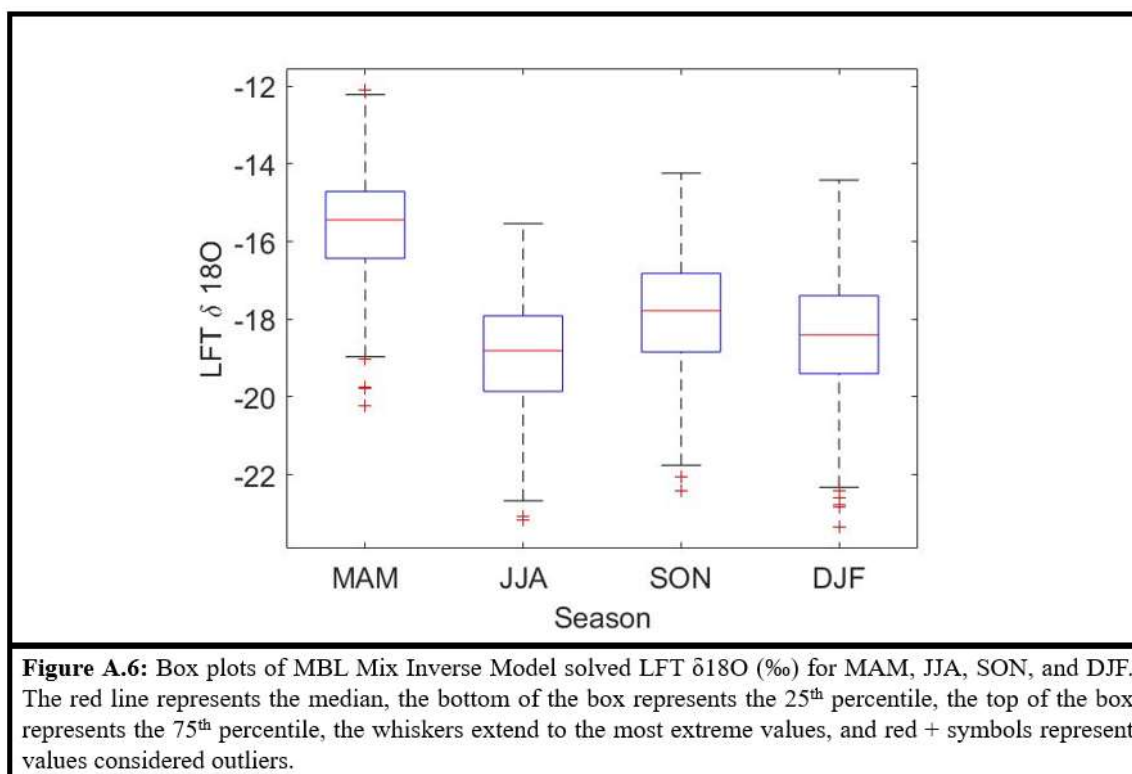
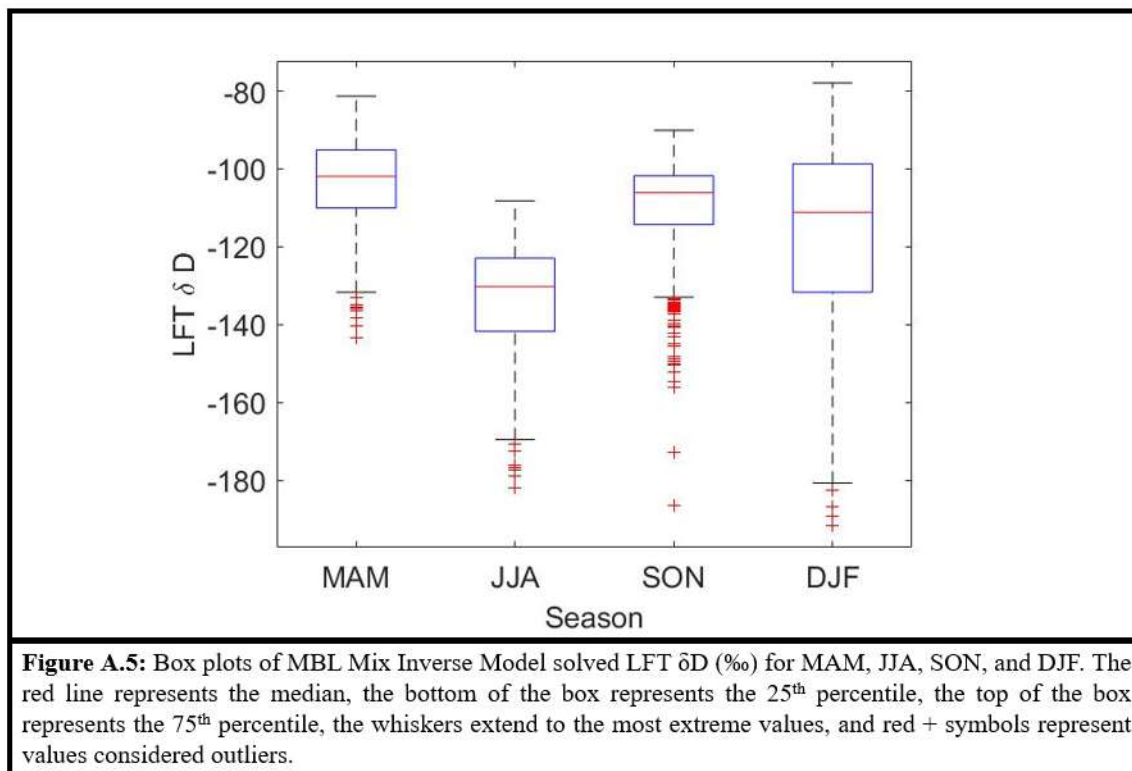


Table A.1: MBL Inverse Model Parameters of Interest									
Rayleigh Fractionation Parameters									
Time Period	Initial $\delta D$ for Rayleigh Fractionation (%)			Initial $\delta^{18}O$ for Rayleigh Fractionation (%)			Lifting Condensation Level (hPa)		
	$\alpha$	$\beta$	Mean	$\alpha$	$\beta$	Mean	$\alpha$	$\beta$	Mean
MAM (2018)	8.83	1.04	-75.1	31.78	10.99	-12.33	4.22	15.03	798.6
JJA (2018)	6.72	1.70	-85.1	25.17	11.49	-13.26	1.06	33.93	757.0
SON (2018)	4.45	0.42	-72.8	24.47	11.82	-13.59	0.73	23.15	757.8
DJF (2018 - 2019)	1.98	0.54	-86.3	27.95	19.00	-14.9	14.08	32.95	819.9
Dry End-Member Parameters									
Time Period	LFT Specific Humidity (g/kg)			LFT $\delta D$ (%)			LFT $\delta^{18}O$ (%)		
	$\alpha$	$\beta$	Mean	$\alpha$	$\beta$	Mean	$\alpha$	$\beta$	Mean
MAM (2018)	16.55	15.50	5.3	-	-	-103.4	-	-	-15.57
JJA (2018)	0.68	19.83	5.9	-	-	-133.3	-	-	-18.92
SON (2018)	7.22	24.29	5.6	-	-	-109.8	-	-	-17.83
DJF (2018 - 2019)	8.52	8.18	5.6	-	-	-117.1	-	-	-18.45
Moist End-Member Parameters									
Time Period	Evaporative Flux Saturation Specific Humidity (g/kg)			Ocean Surface $\delta D$ (%)			Ocean Surface $\delta^{18}O$ (%)		
	$\alpha$	$\beta$	Mean	$\alpha$	$\beta$	Mean	$\alpha$	$\beta$	Mean
MAM (2018)	-	-	12.0	11.24	14.86	4.3	2.08	30.52	0.14
JJA (2018)	-	-	16.8	8.09	10.89	4.2	1.84	34.64	0.10
SON (2018)	-	-	15.8	3.84	10.55	2.7	0.37	38.56	0.02
DJF (2018 - 2019)	-	-	11.8	4.35	21.11	1.7	0.07	30.27	0.01
MBL Parameters									
Time Period	MBL Specific Humidity (g/kg)			MBL $\delta D$ (%)			MBL $\delta^{18}O$ (%)		
	$\alpha$	$\beta$	Mean	$\alpha$	$\beta$	Mean	$\alpha$	$\beta$	Mean
MAM (2018)	-	-	8.0	-	-	-89.9	-	-	-13.3
JJA (2018)	-	-	12.8	-	-	-84.2	-	-	-12.20
SON (2018)	-	-	11.2	-	-	-84.7	-	-	-12.84
DJF (2018 - 2019)	-	-	8.1	-	-	-94.6	-	-	-14.18
MBL Mix Inverse Model Mixing Parameter									
Time Period	LFT Mixing (fraction of mixing)								
	$\alpha$			$\beta$			Mean		
MAM (2018)	0.89			1.05			0.70		
JJA (2018)	1.91			8.21			0.47		
SON (2018)	0.98			2.74			0.53		
DJF (2018 - 2019)	1.51			2.37			0.65		

**Table A.1:** Parameters of interest from the MBL Mix inverse model for each season are reported, which include parameters related to Rayleigh fractionation, the model dry end-member and moist end-member, the MBL, and LFT mixing. For each parameter, the inverse model solved alpha and beta parameters for the beta distributions are reported with the mean of their distributions.







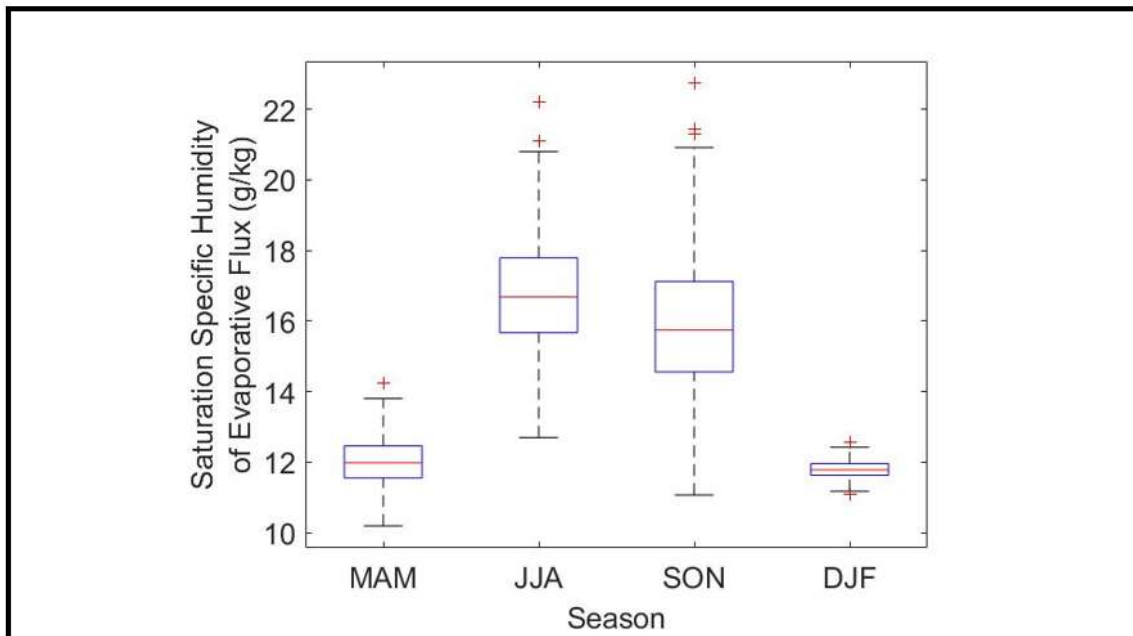


**Figure A.7:** Box plots of evaporative flux saturation specific humidity (g/kg) used in MBL Mix Inverse Model calculated using seasonal SST and surface pressure for MAM, JJA, SON, and DJF. The red line represents the median, the bottom of the box represents the 25<sup>th</sup> percentile, the top of the box represents the 75<sup>th</sup> percentile, the whiskers extend to the most extreme values, and red + symbols represent values considered outliers.

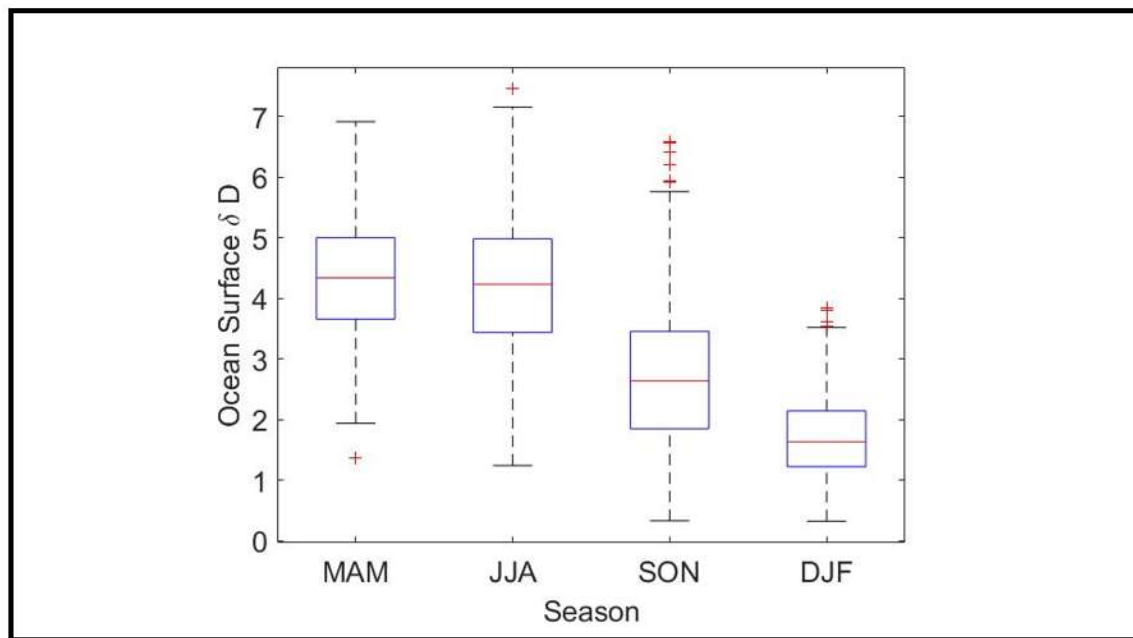


**Figure A.8:** Box plots of MBL Mix Inverse Model solved ocean surface  $\delta D$  (%) for MAM, JJA, SON, and DJF. The red line represents the median, the bottom of the box represents the 25<sup>th</sup> percentile, the top of the box represents the 75<sup>th</sup> percentile, the whiskers extend to the most extreme values, and red + symbols represent values considered outliers.

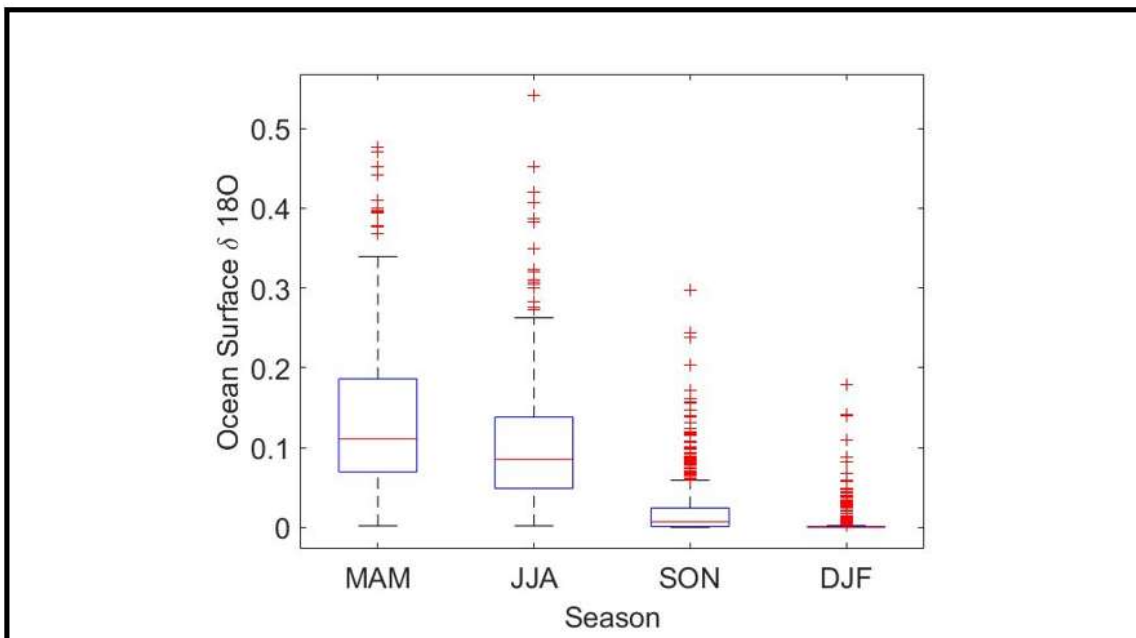


**Figure A.9:** Box plots of MBL Mix Inverse Model solved ocean surface  $\delta 18O$  (%) for MAM, JJA, SON, and DJF. The red line represents the median, the bottom of the box represents the 25<sup>th</sup> percentile, the top of the box represents the 75<sup>th</sup> percentile, the whiskers extend to the most extreme values, and red + symbols represent values considered outliers.

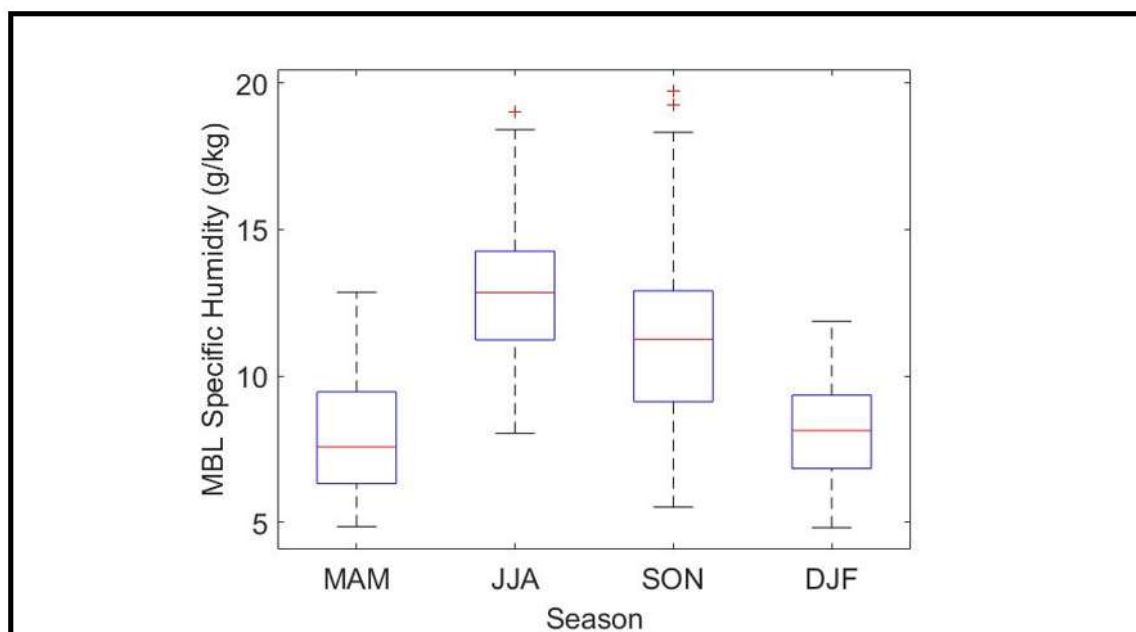


**Figure A.10:** Box plots of MBL Mix Inverse Model solved MBL Specific Humidity (g/kg) for MAM, JJA, SON, and DJF. The red line represents the median, the bottom of the box represents the 25<sup>th</sup> percentile, the top of the box represents the 75<sup>th</sup> percentile, the whiskers extend to the most extreme values, and red + symbols represent values considered outliers.

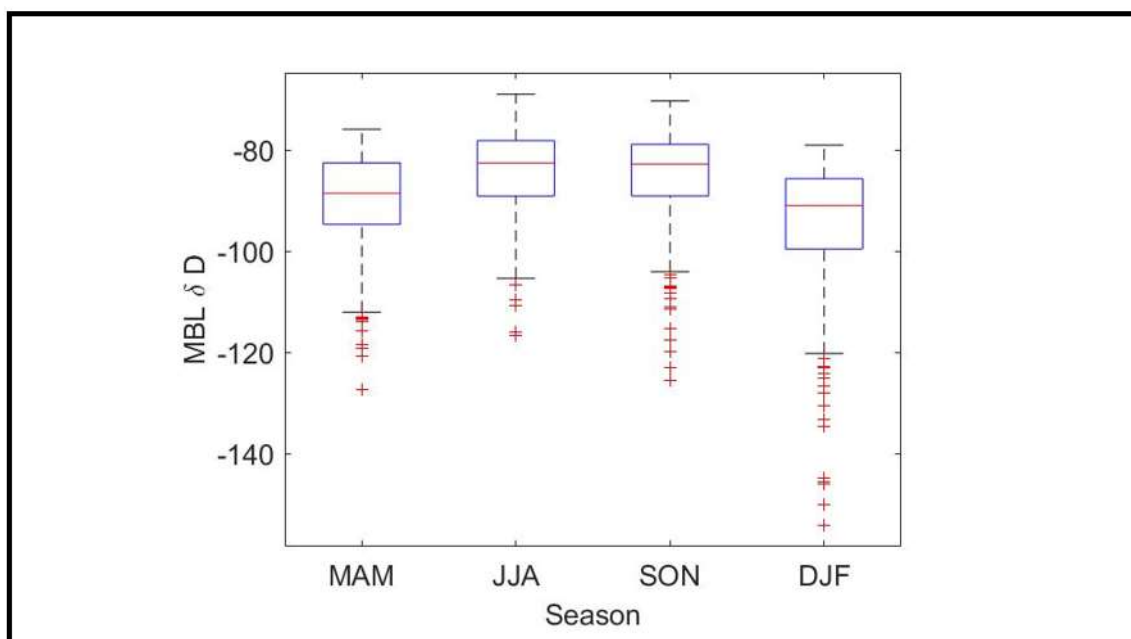


**Figure A.11:** Box plots of MBL Mix Inverse Model solved MBL  $\delta D$  (%) for MAM, JJA, SON, and DJF. The red line represents the median, the bottom of the box represents the 25<sup>th</sup> percentile, the top of the box represents the 75<sup>th</sup> percentile, the whiskers extend to the most extreme values, and red + symbols represent values considered outliers.

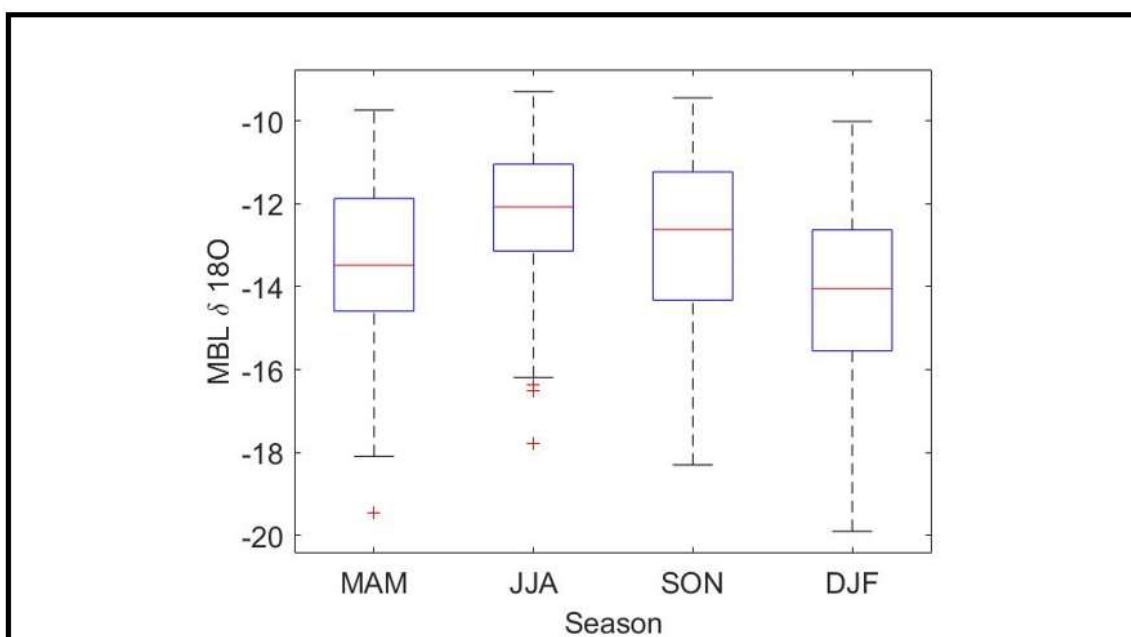


**Figure A.12:** Box plots of MBL Mix Inverse Model solved MBL  $\delta 18O$  (‰) for MAM, JJA, SON, and DJF. The red line represents the median, the bottom of the box represents the 25<sup>th</sup> percentile, the top of the box represents the 75<sup>th</sup> percentile, the whiskers extend to the most extreme values, and red + symbols represent values considered outliers.

## References

- Bailey, A., D. Noone, M. Berkelhammer, H. C. Steen-Larsen, and P. Sato (2015), The stability and calibration of water vapor isotope ratio measurements during long-term deployments, *Atmos. Meas. Tech. Discuss.*, 8(5), 5425–5466.
- Barry, Roger G., and Richard J. Chorley (2010). *Atmosphere, weather, and climate*. Routledge.
- Beasley, D., R. R. Martin, and D. R. Bull, 1993a: An overview of genetic algorithms: Part 1, fundamentals. *Univ. Comput.*, 15, 58–69.
- Beasley, D. R. Bull, and R. R. Martin, 1993b: An overview of genetic algorithms: Part 2, research topics. *Univ. Comput.*, 15, 170–181.
- Benetti, M., G. Reverdin, C. Pierre, L. Merlivat, C. Risi, H. C. Steen-Larsen, and F. Vimeux (2014), Deuterium excess in marine water vapor: Dependency on relative humidity and surface wind speed during evaporation, *J. Geophys. Res. Atmos.*, 119, 584–593, doi:10.1002/2013JD020535.
- Benetti, M., G. Aloisi, G. Reverdin, C. Risi, and G. Sèze (2015), Importance of boundary layer mixing for the isotopic composition of surface vapor over the subtropical North Atlantic Ocean, *J. Geophys. Res. Atmos.*, 120, 2190–2209, doi:10.1002/2014JD021947.
- Benetti, M., G. Reverdin, G. Aloisi, and Á. Sveinbjörnsdóttir (2017), Stable isotopes in surface waters of the Atlantic Ocean: Indicators of ocean-atmosphere water fluxes and oceanic mixing processes, *J. Geophys. Res. Oceans*, 122, 4723–4742, doi:10.1002/2017JC012712.
- Benetti, M., Lacour, J.-L., Sveinbjörnsdóttir, A. E., Aloisi, G., Reverdin, G., Risi, C., et al. (2018). A framework to study mixing processes in the marine boundary layer using water vapor isotope measurements. *Geophysical Research Letters*, 45, 2525–2532. <https://doi.org/10.1002/2018GL077167>.
- Bony, S., and J. L. Dufresne (2005), Marine boundary layer clouds at the heart of tropical cloud feedback uncertainties in climate models, *Geophys. Res. Lett.*, 32, L20806, doi:10.1029/2005GL023851



- Bony, S., C. Risi, and F. Vimeux (2008), Influence of convective processes on the isotopic composition ( $\delta^{18}\text{O}$  and  $\delta\text{D}$ ) of precipitation and water vapor in the tropics: 1. Radiative-convective equilibrium and Tropical Ocean–Global Atmosphere–Coupled Ocean–atmosphere Response Experiment (TOGA-COARE) simulations, *J. Geophys. Res.*, 113, D19305, doi:10.1029/2008JD009942.
- Charney, J. G., A. Arkawa, D. J. Baker, et al. (1979) Carbon dioxide and climate: A scientific assessment. National Academy of Science, 33.
- Craig, H. (1961), Isotopic variations in meteoric waters, *Science*, 133(346), 1702–1703.
- Craig, H., and L. I. Gordon (1965), Deuterium and oxygen-18 variations in the ocean and the marine atmosphere, in *Stable Isotopes in Oceanographic Studies and Paleotemperatures*, edited by E. Tongiorgi, pp. 9–130, V. Lishi e F., Pisa, Spoleto, Italy.
- Dansgaard, W. (1954), The  $\text{O}^{18}$ -abundance in fresh water, *Geochim. Cosmochim. Acta*, 6(5-6), 241–260
- Dansgaard, W. (1964), Stable isotopes in precipitation, *Tellus*, 16(4), 436–468.
- Duan, S. Q., Wright, J. S., & Romps, D. M. (2018). On the utility (or futility) of using stable water isotopes to constrain the bulk properties of tropical convection. *Journal of Advances in Modeling Earth Systems*, 10, 516–529.  
<https://doi.org/10.1002/2017MS001074>
- Galewsky, J. (2018). Using stable isotopes in water vapor to diagnose relationships between lower-tropospheric stability, mixing, and low-cloud cover near the Island of Hawaii. *Geophysical Research Letters*, 45, 297–305.
- Galewsky, J., & Hurley, J. V. (2010). An advection-condensation model for subtropical water vapor isotopic ratios. *Journal of Geophysical Research*, 115, D16116.  
<https://doi.org/10.1029/2009JD013651>
- Galewsky, J., & Rabanus, D. (2016). A stochastic model for diagnosing subtropical humidity dynamics with stable isotopologues of water vapor. *Journal of the Atmospheric Sciences*, 73(4), 1741–1753.

- Galewsky, J., Steen Larsen, H. C., Field, R. D., Worden, J., Risi, C., & Schneider, M. (2016). Stable isotopes in atmospheric water vapor and applications to the hydrologic cycle. *Reviews of Geophysics*, 54, 809–865. <https://doi.org/10.1002/2015RG000512>
- Gedzelman, S. (1988), Deuterium in water vapor above the atmospheric boundary layer, *Tellus, Ser. B*, 40, 134–147.
- Hartmann, D.L. and D.A. Short (1980) On the Use of Earth Radiation Budget Statistics for Studies of Clouds and Climate *J. Atmos. Sci.*, 37, 1233–1250, [https://doi.org/10.1175/1520-0469\(1980\)037<1233:OTUOER>2.0.CO;2](https://doi.org/10.1175/1520-0469(1980)037<1233:OTUOER>2.0.CO;2)
- IPCC (2013) Climate Change 2013: The Physical Science Basis. Contribution of Working Group I to the fifth assessment report of the Intergovernmental Panel on Climate Change [Stocker, T.F., D. Quin, G.-K. Plattner, M. Tignor, S.K. Allen, J. Boschung, A. Nauels, Y. Xia, V. Bex and P.M. Midgley (eds.)]. *Cambridge University Press*, 1535 pp, doi:10.1017/CBO9781107415324.
- Johnson, L. R., Sharp, Z. D., Galewsky, J. , Strong, M. , Van Pelt, A. D., Dong, F. and Noone, D. (2011), Hydrogen isotope correction for laser instrument measurement bias at low water vapor concentration using conventional isotope analyses: application to measurements from Mauna Loa Observatory, Hawaii. *Rapid Commun. Mass Spectrom.*, 25: 608-616. doi:10.1002/rcm.4894
- Jouzel, J., and R. D. Koster (1996), A reconsideration of the initial conditions used for stable water isotope models, *J. Geophys. Res.*, 101, 22,933–22,938, doi:10.1029/96JD02362.
- Kurita, N., D. Noone, C. Risi, G. A. Schmidt, H. Yamada, and K. Yoneyama (2011), Intraseasonal isotopic variation associated with the Madden-Julian Oscillation, *J. Geophys. Res.*, 116, D24101, doi:10.1029/2010JD015209.
- Kurita, N. (2013), Water isotopic variability in response to mesoscale convective system over the tropical ocean, *J. Geophys. Res. Atmos.*, 118, 10,376–10,390, doi:10.1002/jgrd.50754.

- Lacour, J.-L., Risi, C., Clarisse, L., Bony, S., Hurtmans, D., Clerbaux, C., & Coheur, P.-F. (2012). Mid-tropospheric  $\delta\text{D}$  observations from IASI/MetOp at high spatial and temporal resolution. *Atmospheric Chemistry and Physics*, 12(22), 10,817–10,832. <https://doi.org/10.5194/acp-12-10817-2012>
- Lis, G., Wassenaar, L. I., and Hendry, M. J. (2008) High-precision laser spectroscopy D/H and  $^{18}\text{O}/^{16}\text{O}$  measurements of microliter natural water samples, *Anal. Chem.*, 80, 287–293, doi:10.1021/ac701716q.
- Mckinney, C. R., et al (1950) Improvements in Mass Spectrometers for the Measurement of Small Differences in Isotope Abundance Ratios. *Review of Scientific Instruments*, vol. 21, no. 8, pp. 724–730., doi:10.1063/1.1745698.
- Merlivat, L., and J. Jouzel (1979), Global climatic interpretation of the deuterium-oxygen-18 relationship for precipitation, *J. Geophys. Res.*, 84(C8), 5029–5033, doi:10.1029/JC084iC08p05029.
- NOAA High Resolution SST data provided by the NOAA/OAR/ESRL PSD, Boulder, Colorado, USA, from their Web site at <https://www.esrl.noaa.gov/psd/>*
- Noone, D. (2012), Pairing measurements of the water vapor isotope ratio with humidity to deduce atmospheric moistening and dehydration in the tropical midtroposphere, *J. Clim.*, 25, 4476–4494.
- Peacock, J. A., 1983: Two-dimensional goodness-of-fit testing in astronomy. *Mon. Not. Roy. Astron. Soc.*, 202, 615–627, doi:10.1093/mnras/202.3.615.
- Rémillard, J., P. Kollias, E. Luke, and R. Wood, (2012) Marine Boundary Layer Cloud Observations in the Azores. *J. Climate*, 25, 7381-7398, <https://doi.org/10.1175/JCLI-D-11-00610.1>.
- Reynolds, R.W., T.M. Smith, C. Liu, D.B. Chelton, K.S. Casey, and M.G. Schlax, (2007) Daily High Resolution-Blended Analyses for Sea Surface Temperature. *J. Climate*, 20, 5473 – 5496, <https://doi.org/10.1175/2007JCLI1824.1>

- Rieck, Malte, et al. (2012) Marine Boundary Layer Cloud Feedbacks in a Constant Relative Humidity Atmosphere. *Journal of the Atmospheric Sciences*, vol. 69, no. 8, pp. 2538–2550., doi:10.1175/jas-d-11-0203.1.
- Risi, C., Galewsky, J., Reverdin, G., and Brient, F.: Controls on the water vapor isotopic composition near the surface of tropical oceans and role of boundary layer mixing processes, *Atmos. Chem. Phys. Discuss.*, <https://doi.org/10.5194/acp-2019-254>, in review, 2019.
- Santos, F, et al. (2004) Climate Change Scenarios in the Azores and Madeira Islands. *World Resource Review*, 16,473–491.
- Sharp, Z. (2006), *Principles of Stable Isotope Geochemistry*, Prentice Hall.
- Sherwood, S. C., W. Ingram, Y. Tsushima, M. Satoh, M. Roberts, P. L. Vidale, and P. A. O’Gorman (2010), Relative humidity changes in a warmer climate, *J. Geophys. Res.*, 115, D09104, doi:10.1029/2009JD012585.
- Sherwood, S. C., S. Bony, and J.-L. Dufresne (2014), Spread in model climate sensitivity traced to atmospheric convective mixing, *Nature*, 505(7481), 37–42.
- Steen-Larsen, H. C., A. E. Sveinbjörnsdóttir, A. J. Peters, V. Masson-Delmotte, M. P. Guishard, G. Hsiao, D. Noone, J. K. Warren, and J.W. C.White (2014), Climatic controls on water vapor deuterium excess in the marine boundary layer of the North Atlantic based on 500 days of in-situ, continuous measurements, *Atmos. Chem. Phys.*, 14(15), 7741–7756, doi:10.5194/acp-14-7741-2014.
- Sturm, P. and Knohl, A. (2010) Water vapor  $\delta^2\text{H}$  and  $\delta^{18}\text{O}$  measurements using off axis integrated cavity output spectroscopy, *Atmos. Meas. Tech.*, 3, 67–77, doi:10.5194/amt-3-67-2010.
- Wood, R. et al (2015), Clouds, aerosols, and precipitation in the marine boundary layer: an ARM mobile facility deployment. *Bull. Amer. Meteor. Soc.*, 96, 419–440, <https://doi.org/10.1175/BAMS-D-13-00180.1>

Worden, J., Kulawik, S., Frankenberg, C., Payne, V., Bowman, K., Cady-Peirara, K., et al. (2012). Profiles of CH<sub>4</sub>, HDO, H<sub>2</sub>O, and N<sub>2</sub>O with improved lower tropospheric vertical resolution from Aura TES radiances. *Atmospheric Measurement Techniques*, 5(2), 397–411. <https://doi.org/10.5194/amt-5-397-2012>

Yoshimura, K., M. Kanamitsu, D. Noone, and T. Oki (2008), Historical isotope simulation using Reanalysis atmospheric data, *J. Geophys. Res.*, 113, D19108, doi:10.1029/2008JD010074.